Development and Validation of Two-Phase CFD Models for Key Elements of Propellant Tank CFM Operations in 1G and Microgravity – An Overview

M. Kassemi [1] and D. Hauser [2]
[1]*National Center for Space Exploration (NCSER), Case Western Reserve University & NASA Glenn Research Center, Cleveland, Ohio, USA.*

[2]*NASA Glenn Research Center, Cleveland, Ohio, 44135, USA*

O. Kartuzova [3]
[3]*National Center for Space Exploration (NCSER), Case Western Reserve University & NASA Glenn Research Center, Cleveland, Ohio, 44135, USA.*

S. Hylton [4]
[4]*National Center for Space Exploration (NCSER), Case Western Reserve University & NASA Glenn Research Center, Cleveland, Ohio, 44135, USA.*

This paper presents an overview of the state-of-the-art two-phase CFD models that have been developed for various propellant tank storage and transfer operations in 1g, partial gravity and microgravity. The models are developed in the framework of the industry standard ANSYS/Fluent CFD code, the capabilities of which have been significantly enhanced and customized through incorporation of unique submodels via User Defined Functions (UDF)s to satisfy the requirements of its intended variable gravity Cryogenic Fluid Management (CFM) applications. These models/submodels have been validated against experimental data that cross spatial scales, fluid types, and gravity levels in order to properly anchor the models' physical and numerical fidelity. The CFM application/processes that have been modeled include tank self-pressurization, tank autogenous pressurization, tank pressure control using both subcooled jet mixing and droplet spray injection mechanisms, tank chilldown/filling, tank drainage, tank slosh for both volatile and non-volatile fluids. The strength and shortcomings of the two-phase models for each application is highlighted and discussed briefly.

I. Nomenclature

E = energy, J
F = force, N
g = gravitational acceleration, m/s^2

[1] Research Professor, Department of Mechanical & Aerospace Engineering, AIAA Associate Fellow.
[2] Fluids Engineer, Fluid and Cryogenic Systems Branch.
[3] Research Assistant Professor, Department of Mechanical & Aerospace Engineering, and AIAA Member.
[4] Research Scientist, Department of Mechanical & Aerospace Engineering.

h = enthalpy, J/kg
k = thermal conductivity, W/m·K
$\boldsymbol{n}$ = normal vector
p, P = pressure, Pa
t = time, seconds
T = temperature, K
$\mathbf{v}$ = velocity, m/s

Greek

α = cell value of volume fraction
μ = Pa·s
ρ = density, kg/m^3
σ = surface tension, N/m

Subscripts

eff = effective
i = interface
q = phase

II. Introduction

Propellant tanks are subject to various undesirable heat loads while loitering in LEO, in transit, or sitting on the surface of Moon or Mars. The resultant heat leak that passes through the protective passive insulation system into the tank will evaporate the propellant, raise the tank pressure, and ultimately lead to fuel loss when vapor is vented in order to relieve the excess pressure[1]. Transverse temperature gradients generated by the heat leaks will also give rise to natural convection that may be core-driven and weak at low Ra numbers and boundary layer driven and turbulent at high Ra numbers[2]. If this natural convection current is not controlled, it will create significant thermal stratification leading to considerable evaporation at the interface. The natural convection regime and the intensity of the buoyancy-driven flow and heat transfer, as characterized by the tank Ra number, is gravity-dependent. Consequently, there can be large quantitative and qualitative differences between microgravity and 1g thermal stratifications and self-pressurization rates. In space, the position of the liquid-vapor interface is also not well defined and will be influenced by the direction and magnitude of the time-dependent residual gravitational field. The effect of the multiple time scales associated with these convective, transport, and phase change mechanisms have to be all captured, isolated, and characterized by the CFD models with great fidelity in order to properly predict the tank self-pressurization and pressure reduction time constants[2, 3].

Self-pressurization and pressure control of the storage tanks in microgravity are complicated by the complex dynamic interactions among forced mixing, the various gravity-dependent transport mechanisms in the vapor and liquid phases, the condensation-evaporation processes that occur at the moving and deforming vapor-liquid interface and the dominance of surface forces over body forces in weightlessness[3-9]. This complicated underlying physics together with the prohibitive costs associated with a much-needed but elusive large scale on-orbit Technology Demonstration, have created an increased reliance on computational models to provide the required crossing between scales, fluid types, and gravitational levels to guide the future propellant tank designs[2].

A proposed method for controlling and mitigating the thermal stratification is through mixing of the bulk liquid by an intermittent forced jet flow[10-12]. Due to the low viscosity of the cryogenic fluids (e.g., hydrogen, oxygen, and methane) and the large dimensions of the storage tank, both the natural and the forced convection will be turbulent for typical on-surface applications and even in microgravity, for very large tanks[13]. The interaction between the forced jet and the ullage and its effect on destratification and interfacial heat and mass transfer is neither trivial nor intuitive in microgravity.

Another means of controlling the tank pressure is via injection of subcooled liquid droplets through an axial spray-bar[14]. Here, the injected subcooled liquid can promote mixing and destratification in the liquid and condensation at the bulk phases' interface. The droplets that are injected into the ullage can also provide additional cooling of the ullage as they vaporize and extract the required heat of vaporization from the hot vapor. Although promising, this technology has never been tested in microgravity. Various liquid injection mechanisms have also been proposed for tank chilldown and filling operations. Here again, the droplet transport and phase change issues are important and even more complex as the interaction of droplet with a hot wall during the chilldown process must be simulated using two-phase conjugated CFD models[15,16].

During autogeneous tank pressurization[17] for liquid extraction the pressurization of the ullage is accompanied by significant condensation at the bulk vapor-liquid interface creating a relatively thin thermal layer with a sharp gradient in the liquid just below the interface that must be captured by CFD with great fidelity in order to ultimately estimate the amount of gas injection that is required[18]. Again, both gravity and slosh as it affects the interaction of the convective gaseous and liquid flows with the phase front will play important roles in the process.

While ullage movement due to sudden thrust acceleration in space can produce pressure spikes in a stratified tank, liquid slosh due to similar accelerations can lead to vehement oscillation of the interface that can potentially lead to the disintegration of the liquid surface and creation of droplets. The sloshing process can thus promote significant interfacial condensation and droplet evaporation leading to sudden reduction in pressure and ultimately ullage collapse[19-20]. CFD simulations that can predict liquid slosh dynamics in microgravity with and without phase change are thus indispensable in the design of future tanks and mission scenarios[21-22].

In this light, in order to support the on-orbit storage and transfer of cryogenic propellant operations for future Space expeditions, NASA has been investing in improving the predictive capabilities of computational models and CFD codes that will serve as design tools for sizing the equipment and predicting the performance of different propellant storage and transfer strategies. This has created a great reliance on two-phase Computational Fluid Dynamics (CFD) models to help acquire the needed scientific understanding of the interacting phenomena that affect the two-phase heat and mass transfer involved with cryogenic propellants. However, before the CFD models can be fully trusted to perform this important role, they have to be properly validated and verified against 1g and microgravity data, for simulation of each propellant tank operation.

In this paper we present an overview of the two-phase CFD models that have been developed for various propellant tank storage and transfer operations in the framework of the ANSYS/Fluent CFD code that has been customized by in-house developed submodels implemented through User Defined Functions (UDF)s. These models have been validated against experimental data that cross spatial scales, fluid types, and gravity levels in order to properly anchor the models' physical and numerical fidelity. To date, the model development and validations studies have been focused on:

- **Tank Self-Pressurization** where several CFD models have been developed and validated against large scale 1g cryogenic fluid experiments carried out at NASA (MHTB, Ksite, Saturn AS-203, SHIIVER), small scale microgravity experiments using simulant fluids (ZBOT) and medium scale cryogenic fluid experiments in microgravity (RRM3)
- **Tank Pressure Control** with both jet mixing and spray-bar droplet injection operations where CFD models have been developed and validated against large scale, 1g, cryogenic jet mixing experiment (Ksite) and large scale, 1g, cryogenic spray-bar/droplet injection experiment (MHTB) and microgravity small scale simulant fluid experiments (ZBOT).
- **Tank Sloshing** with nonvolatile and volatile fluids where CFD models have been developed and validated against large scale and small, 1g, simulant and cryogenic sloshing experiments (CNES, JAXA)
- **Tank Pressurization and Draining** where CFD models have been developed and validated against large scale, 1g, cryogenic experiment pressurized with like gases (EDU and DLR/University of Bremen)

In this article we focus on the CFM processes listed above and describe the status of state-of-the-art two-phase CFD models that have been developed at Case Western Reserve University and NASA Glenn Research Center (GRC) and validated against several large-scale ground-based and subscale microgravity self-pressurization and pressure control experiments. The validation case studies are presented and discussed based on a color bar chart that relates both the model and the experimental dataset fidelities to the provisions of NASA STD 7009 Document. We hope to cover the CFD models and simulations that address the other important CFM operations in future articles.

III. Computational Modelling Approach

During the ZBOT-1 investigations, two different two-phase CFD models, namely a Sharp Interface, SI-CFD model and a Volume-of-Fluid, VOF-CFD model, were developed to study storage tank self-pressurization and jet mixing pressure control. Both of these models were subjects to comprehensive and detailed model verification and validation campaigns that include validation against the results of ZBOT-1 ground-based experiments[23-24], ZBOT-1 microgravity experiments[25], and large-scale LH2 experiments that were performed in the NASA Ksite[6,12], MHTB[14] and SHIIVER[26] ground-based cryogenic testbed facilities. For a more detailed presentation of the two associated mathematical models, the reader is referred to Kassemi et al[3-4]. In these CFD models, fluid flow and energy transport are described in terms of the continuity, Navier-Stokes, and enthalpy-based energy equations for both phases. The liquid phase is treated as incompressible with constant or variable temperature-dependent properties. The liquid density is allowed to vary linearly with temperature in the momentum equation. The vapor is modeled as a compressible ideal gas. All the

thermo-physical and thermodynamic properties of the fluids required by the models are taken the NIST Chemistry WebBook[27]. Different treatments of the interface as adopted by the sharp interface SI-CFD and VOF-SI models are briefly described below.

A. The Sharp Interface SI-CFD Model

In the Sharp Interface, or SI-CFD, model, the liquid and vapor regions are separated by a sharp, rigid flat or curved boundary that represents the interface. The governing mass, momentum, and energy equations are solved separately for each phase. The two phases are coupled together through the continuity of velocities and mass flow and the balance of shear stresses and energy at the sharp interface. The energy balance at the interface plays a particularly important role in two-phase flow problems. In our formulation, the net difference between the conductive heat fluxes on the vapor and liquid sides of the interface are computed, and in turn determine the energy that is supplied/removed to sustain the interfacial evaporation/condensation processes. The two phases are coupled at the interface through the continuity of velocities and shear stresses, as well as an energy balance performed at the interface boundary that can be written as:

$$|\dot{\boldsymbol{m}}|L = \boldsymbol{q}_{il} - \boldsymbol{q}_{iv}. \tag{1}$$

Here, L, is the latent heat of phase change, $|\dot{\boldsymbol{m}}|$ is the interfacial mass transfer rate, and $\boldsymbol{q}_{il}$,and $\boldsymbol{q}_{iv}$, are respectively the conductive heat fluxes on the liquid and vapor sides of the interface:

$$\boldsymbol{q}_{il} = -k_{eff-l}\boldsymbol{\nabla}T|_l \tag{2a}$$

$$\boldsymbol{q}_{iv} = -k_{eff-v}\boldsymbol{\nabla}T|_v \tag{2b}$$

In the present implementation of the SI-CFD model, the computations of the interfacial mass transfer and interface temperature are accomplished using a kinetics approach where the mass transfer rate is directly computed from the difference between the vapor pressure at center of the fluid cell next to the interface and the saturation pressure at the interface using a kinetics relationship. Schrage[28] has provided a linearized kinetic relationship derived from gas dynamics theory that has been widely used in phase change problems. In our CFD models, we use a version of the Schrage equation that has been slightly modified for a near-equilibrium condition:

$$|\dot{\mathbf{m}}| = \left(\frac{2a}{2-a}\right)\left(\frac{M}{2\pi RT_i}\right)^{1/2}(P_i - P_v) \tag{3}$$

Here, α, is the accommodation coefficient, M is the molar mass of the fluid, R is the universal gas constant and, P_i and P_v , are, respectively, the interfacial and vapor pressures. It is assumed that that $P_i \cong P_{sat}(T_i)$, and P_v is numerically given by the pressure in the computational cell closest to the interface. The Clausius Clapeyron saturation relationship can be used to relate P_{sat} to the interface temperature and provide closure as:

$$\frac{P_{sat(T_i)}}{P_r} = e^{\left[\frac{L}{R}\left(\frac{1}{T_r}-\frac{1}{T_i}\right)\right]} \tag{4}$$

where the subscript, r, refers to reference values.

Eqs 1-4 can now be solved for both the interface temperature and the mass transfer rate. Since mass transfer is assumed to be relatively small for near equilibrium conditions, there is no jump in the liquid-side and vapor-side temperatures at the interface, and the vapor and liquid side temperatures are equal to the interface temperature. Nevertheless, in this formulation depending on the magnitude of the mass transfer rate as predicted by the modified Schrage equation, the temperature of the interface can deviate from the saturation temperature. But previous work[3, 4] has shown that the interface will essentially remain at the saturation temperature when the mass transfer is small, i.e. at near-equilibrium conditions.

In the sharp interface method, the interface is assumed to be rigid with a predetermined nonevolving shape. Thus, a normal stress balance is not needed. Only a normal velocity boundary condition is required, with the normal vapor and liquid flow velocities set as:

$$\mathbf{v}_v \cdot \hat{\boldsymbol{n}} = \dot{\mathbf{m}}_i . \hat{\boldsymbol{n}} \tag{5a}$$

$$\mathbf{v}_l \cdot \hat{\boldsymbol{n}} \approx 0 \tag{5b}$$

The latter is justified due to the large difference between the vapor and liquid densities.

B. The Volume-of-Fluid VO-CFD Model

In the Volume-of-Fluid CFD model, or the VOF-CFD, the interface is allowed to move and deform subject to imposed body and surface forces and the interface shape and position is captured diffusely through the change in volume fraction following the numerical methodology promulgated by Hirt and Nichols[29]. In this case, only one set of governing conservation equations are solved for both phases, together with an evolution equation for the vapor volume (void) fraction, which is used to distinguish between the two phases. The volume fraction, α, is defined in

each cell such that the volume fractions of the two phases sum up to unity. The interface can then be tracked by solving the evolution or continuity equation for the volume fraction of the q^{th} phase (vapor) as:

$$\frac{1}{\rho_q}\left[\frac{\partial}{\partial t}\left(\alpha_q \rho_q\right) + \nabla \cdot \left(\alpha_q \rho_q \mathbf{v}_q\right) = S_{\alpha_q}\right] \tag{6}$$

The volume fraction for the primary phase (liquid) is determined from:

$$\sum_{q=1}^{2} \alpha_q = 1 \tag{7}$$

All of the field variables and properties can then be defined in terms of the volume fraction as:

$$\rho = \sum_{q=1}^{2} \alpha_q \rho_q,\ \mu_{eff} = \sum_{q=1}^{2} \alpha_q \mu_{eff_q},\ k_{eff} = \sum_{q=1}^{2} \alpha_q k_{eff_q} \tag{8}$$

In this fashion, the continuity, momentum, and energy equations, can be solved throughout the domain for the temperatures and velocities in the two phases, with the energy, *E*, treated as a mass-averaged variable that is described in terms of E_q for each phase, based on the specific heat of that phase and its shared temperature:

$$E = \frac{\sum_{q=1}^{2} \alpha_q \rho_q E_q}{\sum_{q=1}^{2} \alpha_q \rho_q} \tag{9}$$

In the VOF scheme, the interfacial energy, momentum, and mass balances are applied via source terms in the diffuse interfacial region, and in this sense the interfacial energy balance described by Eq 1 is only satisfied volumetrically in the cells that are identified as interfacial cells in the region where the volume fraction is subject to a sharp change between 0 and 1 values. For the interfacial energy balance, the kinetic-Schrage approach, which was previously described for the SI-CFD model, is again adopted. For the VOF-CFD model, the evaporation and condensation mass transfer at the interface is accounted for via source terms in the continuity and volume fraction evolution equation by:

$$S_c = S_{\alpha_q} = \dot{\mathbf{m}}_i \cdot \mathbf{A}_i \tag{10}$$

Here, $\dot{m}_i$, is a mass flux vector which is defined by the Schrage equation and, A_i, is an interfacial area density that can be written as:

$$A_i = |\nabla \alpha| \tag{11}$$

where, α, is the volume fraction of the primary phase.

The additional energy that is carried by the mass of the vapor into the ullage region is accounted for through an enthalpy source term in the energy equation. In the present formulation, the surface tension forces at the interface are modeled via the Continuum Surface Force (CSF) model of Brackbill et al.[30] according to which the surface tension force is transformed into a volume force (F_M), which is added as a source to the momentum equation and applied at the interface computational cells.

C. Lagrangian Spray model

A customized Lagrangian Spray model was also incorporated into the ANSYS Fluent CFD code for simulating the pressure control of a propellent tank by a stream of liquid droplets injected into the ullage. This model uses the Fluent's Euler-Lagrange approach, where the vapor phase (ullage) is treated as a continuum by solving the Navier-Stokes equations. The dispersed droplet phase is solved by tracking a large number of particles (sprayed liquid droplets) through the Eulerian fluid flow domains. The droplets exchange mass, momentum, and energy with the fluid phase. The details of the model and its implementation into fluent is available in Kartuzova & Kassemi[15, 31]. In the Lagrangian spray model, the droplet trajectory is calculated by integrating the force balance on the droplet. This force balance equates the droplet inertia with the forces acting on the droplet as:

$$\frac{d\vec{u}_p}{dt} = F_D\left(\vec{u} - \vec{u}_p\right) + \frac{\vec{g}(\rho_p - \rho)}{\rho_p} + \vec{F}, \tag{12}$$

where $\vec{u}$ is the fluid phase velocity, $\vec{u}_p$ is the particle velocity, ρ is the fluid density, ρ_p is the density of the droplet, F_D is the drag force per unit droplet mass, and $\vec{F}$ is an additional acceleration. A time integration of Eq. 12 yields the velocity of the droplet at each point along the droplet trajectory. The spherical drag law proposed by Morsi and Alexander[27] is applied for the droplet drag force calculation.

Due to phase change the droplet energy equation plays an important role and is solved in the user subroutine as:

$$m_p c_{p_p} \frac{dT_p}{dt} = h \cdot A_p\left(T_\infty - T_p\right) - L\dot{m}_p, \tag{13}$$

where m_p is the droplet mass, c_{p_p} is the heat capacity of the droplet, A_p is the surface area of the droplet, T_∞ is the local temperature of the continuous phase, h is the convective heat transfer coefficient, L is the latent heat, and $\dot{m}_p$ is the rate of droplet evaporation or condensation in kg/s.

Two droplet mass transfer models are also developed and implemented into the overall Eulerian-Lagrangian framework. The first is a kinetic-based model in which the rate of droplet evaporation/condensation is obtained from the Schrage relation (Eq. 3). The temperature of the droplet is then obtained from Eq 13. The second model is the T-sat model where the droplet is first allowed to warm up to the saturation temperature corresponding to the tank's vapor pressure, after which it is assumed that all of the energy supplied by the ullage is used by the evaporation process while the droplet remains at its saturation temperature, such that:

$$\begin{aligned} &\text{if } T_p < T_{sat}(P_v) \Rightarrow \dot{m}_p = 0;\ T_p \text{ is calculated from Eq. (13)} \\ &\text{if } T_p \geq T_{sat}(P_v) \Rightarrow T_p = T_{sat}(P_v);\ \dot{m}_p \text{ is calculated from Eq. (13)} \end{aligned} \tag{14}$$

In this case, the evaporation rate can be calculated directly from the droplet energy balance (eq. 13).

In both models, a correlation of Ranz and Marshall[32-33] is used to evaluate the droplet heat transfer coefficient:

$$Nu = \frac{hd_p}{k_\infty} = 2.0 + 0.6Re_d^{1/2}Pr^{1/3}, \tag{15}$$

where d_p is the droplet diameter, k_∞ is the thermal conductivity of the continuous phase, Re_d is the Reynolds number based on the particle diameter and the relative velocity, and Pr is the Prandtl number of the continuous phase. Here, the relative Reynolds number is calculated as:

$$Re_d \equiv \frac{\rho d_p \left|\overrightarrow{u_p} - \vec{u}\right|}{\mu}, \tag{16}$$

where μ is the molecular viscosity of the fluid. After the droplet energy equation is solved in the user subroutine, the mass, diameter, and temperature of each droplet can be updated.

The mass, momentum, and energy transfer between the droplets and the continuous phase is modeled via source terms. The Lagrangian Spray model is coupled with the VOF-CFD model via a user subroutine that performs particle tracking in the ullage, removes particles from the ullage when they reach the interface, and then adds their contributions to the liquid mass, momentum, and energy equations through source terms. These source terms are added to those liquid cells at the location where the spray drops cross the liquid-vapor interface. Because the VOF method produces a diffuse interface, the criteria for determining when the spray drops have crossed into the bulk liquid is defined as the liquid drop entering a fluid cell with a liquid volume fraction > 0.1.

IV. Results & Discussion

An overview of key CFD model validation and verification work that has been performed, to date, at the National Center for Space Exploration Research (NCSER) at NASA Glenn Research Center (GRC) and Case Western Reserve University (CWRU) is presented in this section. All CFD simulations were performed using an in-house customized version of Ansys/Fluent CFD code as described previously. First, we will consider propellant tank storage and begin with presentation of four large cryogenic (Liquid Hydrogen, LH2) tank self-pressurization cases and one small simulant fluid (Perfluoro-n-Pentane, PnP) validation study. The experiments were all performed at NASA experimental facilities.

A. The 1G Tank Self-Pressurization Validation Studies

The first set of benchmark experiments considered for model validation were performed in the K-site facility at NASA Glenn Research Center[6-7]. The tank, in this case, is a flight-weight aluminum ellipsoidal enclosure with an internal volume of 4.95 m^3 as shown in Fig 1a. It was insulated with two Multi-layer Insulation (MLI) blankets. Self-Pressurization tests were performed from a stratified state in a cryo-shroud with 2 and 3.5 W/m^2 heat loads. The pressurization and pressure control results of these experiments have been used to validate and verify our two-phase Storage Tank CFD models as described in detail in previous papers[3,4,13].

The VOF conjugated turbulent and laminar CFD models that include coupling between wall conduction and the CFD computations are used for these axisymmetric simulations. The predicted self-pressurization rate for the case where 3.5 W/m^2 heat load is applied to the outer tank wall boundary are presented in Fig 1c. The results generated by the conjugated VOF_CFD model for this high Ra and high Bo number case [$Ra_L = 1.65(10)^{14}$, $Ra_V = 1.74(10)^{13}$, $Bo = 1.78(10)^6$] are shown for both laminar and turbulent simulations and compared against the measured pressure rise data plotted as solid circles. It is clearly evident that the turbulent analysis under-predicts the experimental pressure rise by

a considerable margin. In contrast, the laminar conjugated simulation provides a quite good agreement with the measured self-pressurization rate. It seems that the laminar analysis captures the overall energy distribution in the tank with better fidelity.

The corresponding laminar and turbulent temperature fields in the K-site tank are shown in Fig. 2d and 2e, respectively. The turbulent model simulation predicts an increased level of mixing that produces more uniform temperatures in both the liquid and ullage regions compared to the laminar simulations. The effect of turbulence in the vapor region is more pronounced where due to turbulent mixing and transport, the extent of ullage stratification predicted by the turbulent model is almost 40% less than those predicted by the laminar model.

The evolution of temperature with time at two locations in the vapor and liquid regions as predicted by the turbulent and laminar simulations are compared to their experimental counterparts in Figs. 1f and 1g. It is clear from the results in Fig. 1f that the turbulent model under-predicts the vapor temperature while the laminar model agrees quite closely with the measurement. Surprisingly, Fig. 1g shows the opposite holds true for the temperature in the liquid region. Here, the turbulent model agrees well with the point temperature measurement while the laminar model noticeably under-predicts the experimental results. The temperature trends in Fig. 1 seem to indicate that the laminar model captures the heat transport in the ullage fairly well while the turbulent model provides a fairer estimate of mixing and heat transfer in the liquid region.

The lack of fidelity of the turbulent model in predicting the measured pressurization rate can be explained as follows. In the turbulent model predictions due to the vigorous turbulent mixing in the ullage it can draw a larger portion of the imposed heat through the wall into the vapor domain. This heat does not remain in the ullage and due to the strong turbulent transport in the vapor and the large effective turbulent conductivities at the interface, a large portion of this heat reaches the interface. As a result, in the turbulent simulations the extent of thermal stratification in the vapor side is relatively low. A sizable portion of the energy reaching the interface from the vapor side is used to supply the heat of evaporation at the interface. The net result is that in the turbulent simulations relatively small energy drawn from the wall remains on the vapor side causing reduced thermal stratification and hence the under-prediction of self-pressurization rate compared to the experiment.

The reason for turbulent model's poor predictions seem to lie at the interface. An examination of the vapor and liquid side effective thermal conductivities at the interface for the laminar and turbulent models suggest that turbulent thermal conductivities are significantly larger than their molecular counterparts. This allows for overprediction of heat leaving the vapor phase. In reality the interface can dampen turbulence significantly and reduce the effective thermal conductivities at the interface. Unfortunately, the current implementation of the RANS model does not include this interfacial damping of turbulent energies. Thus, it seems, that the lack of the fidelity of the turbulent VOF model in predicting the tank pressurization rate and thermal stratification is due to the absence of an empirically based turbulent "law of interface" in the current implementation of the RANS turbulent model within the VOF scheme. In this case, the laminar VOF model seems to be providing a better assessment of energy transport across the interface and in the ullage region based on the use of molecular conductivities at the interface.

Two other 1g large tank cryogenic validation studies are presented next. The first test was performed in the Multi-Purpose Hydrogen Test Bed (MHTB) facility at NASA Marshall Space Flight Center (MSFC)[14], the case examined here, corresponds to a 50% fill level and subject to a non-uniform heat flux distribution of 15.35 W (0.89873 W/m^2) in the un-wetted section and 35.65 W (2.0841 W/m^2) in the wetted surface[15]. This distribution was determined based on thermal desktop calculations that were anchored to the experimental measurements and performed before the CFD simulations. The model validation results for MHTB self -pressurization are presented in Fig. 2. In this case since the nonuniform heat flux into the tank was available and directly imposed on the inner tank wall, there was no need for a conjugated heat transfer analysis. The pressure results for the laminar simulation in Fig 2b indicate excellent agreement with the experimental pressure evolution in both the magnitude and the rate of pressure rise while turbulent simulations again display a pronounced underprediction of the pressurization rate. The vapor temperature comparisons in Fig 2c indicate good agreement between the laminar prediction and the experimental measurement while the turbulent model again underpredicts the ullage thermal stratification severely. This is also reflected in the laminar vs turbulent comparisons of temperature contours in Fig 2d. In short, the MHTB validation results reiterates the findings of the K-site validation case study.

The second test was performed in the Structural Heat Intercept, Insulation, and Vibration Evaluation Rig (SHIIVER), a large-scale cryogenic fluid management (CFM) test bed designed to scale CFM technologies for inclusion on large, in-space stages[26]. The SHIIVER tank has a 4 m internal diameter and a height of 3.3 m and is configured with forward and aft structural heat shield skirts as shown in Fig 3a. For model validation inputs, heat fluxes on the outside of the tank wall which considered heat transfer in the forward and aft skirts and MLI insulation on the domes were calculated in a separate Thermal Desktop Model, as shown in Fig. 3b, and applied as boundary conditions in CFD. This nonuniform heat flux distribution was imposed directly on the outer tank wall in the

conjugated CFD simulation. In this validation study the predictions of both the Sharp Interface and the VOF CFD models were compared to experimental results[34]. Initial tank pressure was set to the measured value of 20 psia (137,895.1 Pa). Experimental fluid temperatures before the beginning of self-pressurization test were used to obtain initial temperature conditions for CFD runs and an initial fill level of 66.37% was used.

As shown in Fig 3c, the laminar simulations with both the SI-CFD and VOF-CFD provide excellent agreement with the experimental pressurization rate and magnitude of the pressure rise. The Turbulent VOF model again underpredicts the pressure evolution significantly as was the case with K-site and MHTB. This similarity is also evident from the laminar and turbulent temperature contours in the tank at the end of self-pressurization as shown in Fig 3d. But, interestingly, the SI-CFD turbulent model seems to also provide a good prediction of the experimental pressurization rate and an acceptable prediction of the magnitude of the tank pressure rise in the SHIIVER tank as displayed in Fig 3c. While the SHIIVER VOF self-pressurization results, shown in Figs. 3c and 3d, are consistent with the results of both K-site and MHTB, the better predictions provided by the turbulent SI-CFD model over the turbulent VOF-CFD model seems to be due to the imposition of turbulent wall condition at the interface in the SI-CFD model. This is in conformity with the explanation presented above for the K-site case. That is, the imposition of wall condition at the interface in the SI_CFD model dissipates turbulence at the phase front, while, in the VOF model, turbulence is not dissipated in the interface region and as a result of higher turbulent effective conductivities, interfacial heat transfer is overpredicted by the VOF-CFD model.

Finally, in crossing scale and fluid type we present self-pressurization model validations against the ground-based results of the Zero-Boil-Off Tank (ZBOT) Experiments[3, 35], a series of small-scale tank pressurization and pressure control science experiments that were performed both in 1g and aboard the International Space Station (ISS) in 2017. The experiment uses a transparent volatile simulant fluid, Perfluoro-n-Pentane (PnP, or C5F12), in a transparent acrylic sealed tank with the goal of delineating the various fluid flow, heat and mass transport, and phase change phenomena that control storage tank pressurization and pressure control in microgravity. ZBOT self-pressurization tests were conducted under three modes: VJ heating, strip heating and simultaneous VJ and strip heating in attempt to simulate heat leaks from the environment, the support structure and both. In this paper, we will only present the 1g vacuum jacket heating case that corresponds more closely to the large-scale experiments presented previously where the tank is heated by global heating from the surroundings.

The results of validation of the SI-CFD against the ground-based results of the vacuum jacket heating self-pressurization experiment performed in the ZBOT flight hardware tank set up is shown in Fig 4. The tank is at a 70% fill-level. In this case the tank is self-pressurized as it is heated by the temperature controlled vacuum jacket that maintains a constant 1K temperature difference between the integrated average jacket and tank wall temperatures throughout the test. The ZBOT flight hardware has very good thermal initial and boundary condition control and subject to stringent preconditioning requirements. Here we are in a high Bo number – moderate Ra number regime [$Ra_L = 9(10)^{10}$, $Ra_V = 7(10)^7$, $Bo = 1.9(10)^4$]. In the light of what we discussed before for Ksite, MHTB, and SHIIVER, in this case, we use a laminar flow model to simulate a truly laminar flow situation. Simulations were performed from uniform conditions established during a preconditioning period. The temperature and flow field in the tank and within the vacuum jacket after 12 hrs. of self-pressurization are shown in Fig. 4b. The corresponding predicted tank pressure evolution with time is compared to its experimental counterpart in Fig 4c. The results indicate that the agreement between the laminar model's prediction and the experimental data for a truly laminar case is excellent. Comparisons were also made between the predicted average tank wall temperature and local fluid and wall temperatures at 10 RTD locations (indicated in Fig 4a) and their experimental counterparts several of which are shown in Fig 10d-h. Again, the agreement between model predictions and experimental data is excellent.

B. The 1G Tank Pressure Control Validation Studies

Two ground-based tank pressure control model validation cases are presented next. Here, experiments using two very different pressure control designs, namely, the subcooled jet mixing and the spray-bar droplet injection mechanisms are considered as benchmark tests. We first examine the 1g LH2 K-site subcooled jet mixing tests[11, 12]. The results presented in Fig 5 are for a 1g pressure control test with an initial tank pressure of 187 Kpa, an initial fill level of approximately 86%, a jet velocity of 1.32 m/s ($Re_{jet} = 160{,}000$)[13]. In the simulations, the gravitational vector is aligned with the tank's central axis in the negative axial direction. A uniform heat flux of 4.2 W/m2 was applied at the tank wall to match the average wall heat flux of the experiment. Conduction through the tank wall was not considered since pressure drop in the tank is mainly dominated by heat removal and destratification by the liquid jet. The initial state of the tank just before the pressure control simulations were obtained from previous self-pressurization simulations that were also validated by experimental results. A comparison of the tank depressurization predictions by the SI-CFD and VOF -CFD models against experimental results for this pressure control test is presented in Fig 5b and again points to the importance of interfacial turbulence on the evolution of tank pressure during the thermal

destratification and interfacial condensation processes caused by the liquid jet mixing. In the VOF simulations, in absence of a rigorous turbulent "law of the interface" condition, a numerical turbulence dampening mechanism was used to dissipate the turbulence in the interfacial region to various degrees. From the results presented in Fig 5b, it is evident that the SI-CFD that applies a law of the wall turbulent condition at the interface under-predicts the initial depressurization rate significantly. On the other hand, the CFD-VOF model without any interfacial turbulence dampening over-predicts the initial experimental. However, the CFD-VOF Scheme with turbulence dampening coefficient of 100 was able to predict the tank pressure drop with great fidelity compared to the experimental results. All the CFD simulations and the experiment indicate that the pressure in the tank settles to the same level of 132 kPa after about 1300 seconds of mixing. The significant effect of interfacial turbulence dampening on the tank thermal destratification during jet mixing can be assessed from the velocity, temperature, and turbulent kinetic energy fields, at t = 1500 secs, displayed in Fig 5c and 5d.

In the second ground-based pressure control validation case, we focus on the MHTB LH2 experiment where the droplet injection spray-bar mechanism commonly used with a Thermodynamic Vent System (TVS) was used as the mechanism for tank pressure control[14]. In this case, unlike for the previous jet mixing phenomena, bulk condensation that occurs at the interface plays a secondary role and the main cause of pressure drop in the tank is evaporation of liquid droplets injected into the ullage. The geometry of the tank including the spraybar used for droplet injection and a schematic of the 3D computational grid are shown in Figs 6a and 6b. Two different droplet phase change models[15, 31, 35-36], that were described in the preceding section, were validated against the experimental MHTB results as displayed in Figs 6c. From Fig 6c, it is evident that the Tsat droplet phase change model provides an excellent prediction of the rate and magnitude of the pressure reduction in the tank compared to the experimental results. The Schrage droplet phase change model, however, significantly under predicts the depressurization rate. In this simulation an accommodation coefficient of 0.01 was used in the Schrage mass transfer equation. We have shown that the magnitude of the evaporative mass flux calculated by the Schrage equation is quite sensitive to the value of accommodation coefficient and that this parameter can be used to effective tune the model to fit the experimental depressurization curve[15]. The superiority of the T-sat droplet phase change model is due to the fact that it agrees with experimental results without the need to set any arbitrary tuning parameter. In addition, Fig 6d indicate that in the VOF-CFD simulations, the droplets remain always at or below the saturation temperature or evaporate using the Tsat model. However, in using the Schrage model simulation, it is apparent that the droplets can reach a super heat of around 10 degrees which is intuitively improbable. Finally, Fig 7 indicates that both of the droplet phase change models seem to capture the experimental temperature evolution in the tank rather well with the Tsat model having a slight but noticeable edge[15, 31].

C. The 1G Autogenous Tank Pressurization and Liquid Extraction Validation Studies

Validation of the SI-CFD and VOF-CFD against the results of the autogenous tank pressurization and draining experiments performed in the Engineering Development Unit (EDU) Test Stand 300 at NASA Marshall Space Flight Center (MSFC) are presented next[18]. In the EDU tests a 150 ft^3 propellant tank was filled with liquid nitrogen (LH2) and pressurized both autogenously by gaseous nitrogen and also by using helium gas as pressurant while using both exposed (in the ullage) and submerged diffuser configurations were tested[17]. In the present validation case only autogeneous pressurization with the unsubmerged diffuser is presented. The experimental the tank is approximately 1.7 m in diameter and has an estimated volume of 4.287 m^3 made out of 6 mm thick aluminum as shown in Fig 8a. The tank is wrapped in Multi-Layer Insulation (MLI). During the draining portion of the test the diffuser was turned off and liquid N2 was drained through the Screen Channel Liquid Acquisition Device. The tank was equipped with temperature sensors on a vertical rake, horizontal rake and on the tank wall.

The case considered here considers a nearly adiabatic tank at an initial fill level of 26% and at uniform initial conditions with T_initial = 77.35 K and P_initial = 101270 Pa. Axisymmetric conjugated VOF and Sharp interface simulations were performed using the computational grid shown in Fig 8b. Tank pressures ecolutions predicted by the SI-CFD model are presented first and compared with the experimental results in Fig 8c . The comparisons include the predictions of both laminar and turbulent models with interfacial phase change and the laminar simulations results without phase change. It is ecident that both the turbulent and laminar SI-CFD models predict very similar tank pressures which match the experimental pressure rise rather well. The model without phase change (No-MT) overpredicts tank pressures compared to the models with phase change and experimental data. This is to be expected since as pressure rises and liquid becomes subcooled compared to the saturation temperature, condensation ensuse at the interface lowering the tank pressure. This condesation influence is absent in the no mass transfer case and leads to the pressure overprediction. The local temperature predictions of the laminar SI-CFD model at specific temperature sensor locations are shown in Fig. 8d and comapred to their experimental counterparts. Results show very good agreement between the predicted and measured values near the center and lower portions of the tank and relatively

larger disagreements for locations at the top near the diffuser. This could have been expected since the heat transfer characteristics of the diffuser where not included in the CFD models.

Next Tank pressure evoluton predicted by the laminar SI-CFD and VOF-CFD multiphase models during pressurization are compared with the experimental data in Fig. 8e. It seems that both models predict very similar tank pressure increases that are in an exelllent agreement with the experiemntal data and within 2.5% of the experimental values, as shown in Fig. 8e. Temperatures and streamlines in the tank at 1600 seconds after the beginning of pressurization are compared between the VOF and Sharp Interface models in Fig. 8f. Both models indicate that hot diffuser flow is mainly rises and mixes with the fluid in the top of the vapor region, while the rest of the vapor region becomes stratified, and the liquid region remains relatively unaffected. Streamlines show mixing happening in the ullage, which helps to slowly bring warmer temperatures from the top of the tank (near the diffuser) towards the interface. The Sharp Interface model predicts two separate recirculation zones in the liquid – one near the interface and another one at the bottom of the tank. In the VOF model these recirculation zones are less distinct.

Finally, validation of tank pressure predictions by the SI-CFD and VOF-CFD against the EDU liquid extraction data is shown in Fig 8g. In this case, the capability of the SI-CFD model was enhanced to allow for the movement of the sharp interface along the longitudinal axis of the tank. As is evident in Fig 8g, both the modified SI-CFD model and the VOF-CFD models predict the rate of the tank pressure decrease well in comparison to the experimental data. Still, in the first 100 seconds of draining, the CFD models are predicting slower pressure drop compared with the experiment. This may be because, in the experiment, the tank was pressurized and the valve was closed right before the draining portion started, but in the CFD simulations this portion of the test was not included. The effect of pressurization prior to draining can influence the interfacial condensation mass transfer and, therefore, the tank pressure. Both models, predict tank pressures reduction rates during liquid extraction that are within 3.5% of the measured values[18].

D. The 1G Tank Slosh Validation Studies – Volatile and Non-Volatile Fluids

Two validation case studies were performed for a tank in 1g where the fluid goes through s relatively strong slosh in response to an imposed forced lateral acceleration. In the first case, the fluid is Silicone Oil. Since this is a nonvolatile fluid, there is no phase change during the slosh cycle. In the second case, the fluid is liquid Nitrogen and goes through phase change at the interface during the slosh period. Both experiments were performed by University of Tokyo[19, 20] and shared with NASA during a NASA-JAXA model validation collaboration.

Two-phase flow and heat transfer simulations of the silicone oil sloshing experiment by Himeno et al.[19] in normal gravity were conducted using the VOF- CFD model. The simulations presented here represent the highest level of lateral acceleration tested in the experiment with a value of 0.5 G. The simulations were performed with and without the tank wall[21]. The later included a conjugate heat transfer analysis. A comparison of simulation results in Fig 9a illustrate the inability of the model without the tank wall to predict pressure increase in the tank at the end of sloshing that occurs mainly due to heat transfer from a warmer wall to a cooler gas. This underscores the importance of a conjugate heat transfer analysis in sloshing studies. The effect of turbulence modeling was also investigated. Here, the predictions of a *Reynolds Averaged Navier-Stokes* (*RANS)* turbulence model and those of a *Large Eddy Simulation* (*LES*) model were compared to the experimental slosh results. Comparisons in Fig 9a indicate that the *LES* approach follows the experimental trends noticeably better than the RANS model, especially, since it captures with good fidelity the change in the rate between the first and second pressure drops at around 0.75 secs in addition to the final increase in pressure that is greatly influenced by wall heat transfer as captured by the conjugated analysis. These results underscore the fact that, at this value of lateral acceleration, the initial temperature conditions in the tank wall have a lesser effect on the tank pressure evolution during sloshing, compared to the effect of turbulence and wall conduction. Thus, appropriate turbulence models are needed together with conjugated heat transfer simulations in order to predict the sloshing behavior of propellant tanks at moderate to high accelerations.

Our next validation study examines the two-phase flow and heat transfer with phase change during the university of Tokyo's Liquid Nitrogen sloshing experiments in normal gravity[20]. The simulations were again performed with the VOF-CFD model with both LES and RANS turbulence submodels[22]. The validation case study considered two different experimental cases with different thermal stratification thickness at the liquid side of the interface. The effects of turbulence modeling, initial wall temperature profiles and the accommodation coefficient on the tank pressure evolution were investigated. The results of these simulations presented in Figs 9c and 9d indicate good agreement with the experimental results especially with regard to the extent of the rapid pressure drop. It also showed that while turbulence modeling approach does not have a significant effect on predicting the tank pressure, the effect of initial conditions and the value of accommodation coefficient that controls interfacial mass transfer play a significant role.

E. The Microgravity Tank Self-Pressurization and Jet-Mixing Pressure Control Validation Studies

We start the microgravity validation cases with the large-scale LH2 Saturn S-IVB AS-203 Space Demonstration that flied in 1966 and was able to conduct a self-pressurization experiment under a time-dependent acceleration field that varied between (3.7e-4 to 8e-5 g)[38,39]. The domed cylindrical tank had a radius, r = 3.3 m, and a height, h = 11.3 m and test was performed at a fill level of 32% with an initial tank pressure of 12.4 psia (85495 Pa) and with the liquid initially at a uniform temperature of 19.72 K and the ullage at an initial superheat of roughly 2.44 K. Due to the large dimensions of the tank that resulted in a Bond number ranging from 43.5 – 145 due to the varying thruster acceleration, the liquid was essentially in a settled configuration for the entire duration of the self-pressurization test. The self-pressurization test examined here did not take place under normal tank operations. Due to insulation failure a large amount of heat (approximately 30,000 W) was imparted on the tank. This is equivalent to a heat flux of about 150 W/m2. Comparing this value to the nominal operational heat load of 3.4 W for K-site tank, it becomes apparent that the self-pressurization of the Saturn tank took place under severely off-nominal conditions due to the insulation failure.

The predictions of the VOF-CFD model[40] for the Saturn IB AS-203 self-pressurization is presented in Fig 10a and compared to both the experimental results and to the numerical predictions by Grayson et al.[41] generated by a Flow3D CFD model. Fig 10a shows the pressure evolution in the tank as a function of time. Unfortunately, due to certain malfunctioning, the microgravity pressurization data is available only for limited durations in the beginning and end of the self-pressurization tests. Nonetheless the excellent agreement between the fluent-based VOF-CFD model with the experimental data and its noticeable edge over the Flow3D predictions is evident. Figs10c shows a comparison between the predictions of flow and thermal stratification in the tank by the Fluent and Flow3D models. The CFD results agree favorably with each other while it seems the Flow3D results predicts a stronger flow near the axis of the tank that may be due to the numerical limitations created by the axis of symmetry.

In Fig 10b VOF-CFD model predictions with and without interfacial phase change mass transfer are compared to the experimental results. The two predictions are on top of each other and precisely follow the experimental trend. It seems that mass transfer at the liquid/ullage interface has a negligible effect on the tank pressure rise for this experiment due to the relatively large wall heat fluxes that is directly imparted to the vapor in S-IVB LH2 tank. Consequently, most of the pressure rise occurs as a result of direct heating of the ullage. This is not the case for operation of most propellant tanks in microgravity. Since due to effective insulation system and heat shields propellant tanks typically receive about two orders of magnitude less heat directly from the environment. Under nominal operational conditions, due to the low thermal inertia of the vapor compared to the liquid, pressure rise in the tank is mostly influenced by the interfacial phase change mass transfer and not by direct heating of the ullage. Thus, while Saturn S-IVB experiment constitutes a large tank cryogenic tank experiment in Space, its pressurization data is not suitable for validating the CFD models as it does not correctly represent the role of interfacial phase change mass transfer that is the main contributor to tank self-pressurization under normal Space conditions.

The Tank Pressure Control Experiment (TPCE)[42, 43] is the second microgravity experiment that was used for validation of the VOF-CFD model for prediction of both tank self-pressurization and pressure control in microgravity[44, 45]. This experiment flew on the Space Shuttle in 1991 (STS-43) and utilizes a small scale transparent acrylic cylindrical tank consisting of a cylindrical section with a 0.254 m in diameter capped by two hemispherical domes as shown in Fig 11a. It is partially filled with a simulant fluid (Freon-113) to about 83 percent by volume. Two heaters were installed inside the tank for self-pressurization experiments, one at the top of the dome opposite the nozzle (Heater A) and one at the center of the tank near the wall (Heater B). The residual gravitational vector points away from Heater B. Heater B was not active during the test run simulated here while the heat flux generated by Heater A was about 1kW/m^2. Values of gravitational acceleration were measured and reported for the TCPE. They indicate several prominent spikes. Unfortunately, the average value of the reported residual axial gravitational acceleration was judged to be unreliable since it is significantly higher than typical microgravity values expected in the shuttle. Nevertheless, the indicated direction of the residual acceleration vector has the tendency to push the ullage towards the top heater and the position of the bubble relative to the top heater has a significant impact on the evolution of the ullage pressure in the tank.

The TPCE test 11 self-pressurization run is subject of the microgravity validation case study here[49]. It was performed with the tank at a fill level of 83% heated only by the top heater from an initial uniform state with T_o = 296 K and P_o = 41.164 kPa. For the validation case presented here, we consider a constant baseline gravitational acceleration in the axial direction equal to $9.81(10)^{-6}$ m/s^2 and an initial ullage location near the top heater. This implies that the experiment was performed in a relatively low Ra number low Bo number regime [Ra_L= $2.7(10)^6$, Ra_V = $2.23(10)^7$, Bo = 0.014].

Simulations were performed with our 3D VOF-CFD model. Fig.11 b shows a comparison between predicted and measured tank pressures during self-pressurization for this case. The corresponding 3D ullage shape and position and the temperature contours and pathlines colored by velocity magnitudes at the tank center plane are presented in Fig.

11d-f for three different time sequences. It is evident from Fig 11b that the model predicts a rapid and steep pressure rise within the first 60 seconds of self-pressurization followed by a decline in the slope of the pressure curve that remains constant for the rest of the self-pressurization period. This can be explained by the heating of the ullage and the mass transfer at the interface as displayed in Fig. 11c. In the first 60 seconds, the heat and evaporative mass flux generated at the vapor interface that is pressed against the top heater propagates into the ullage as shown in Fig 11d. This raises the ullage temperature and pressure drastically, as shown in Fig. 11b. After 60 seconds, the heat reaches the bottom portion of the ullage interface (see Fig. 11e&f) and promotes heat flow into the subcooled liquid and condensation across the lower section of the interface thus lowering the net total mass transfer (integrated over the whole interface) into the ullage. This alters the pressurization rate as indicated by a decline in the slope of the pressure curve starting at around 100 seconds in Fig 11b. Even though in this case, the tank pressure is over-predicted at all times, the computed slope of the pressure curve matches the experiment adequately between the 350- and 500-seconds interval.

It is important to note that the tank in this experiment was not insulated inside the getaway special container where it was installed. Neither the heat loss through the tank wall nor the wall temperatures were measured and reported in ythe experiment. Therefore, the boundary conditions on the tank wall are uncontrolled and unknown. In the absence of relevant information, adiabatic wall boundary conditions were employed in CFD model. This difference between CFD model and experiment allows only for a qualitative comparison and might be responsible for over-prediction of the pressurization level due to the heat loss that was not accounted for in the model, especially, at the wall boundary near the top heater.

Validation of the VOF-CFD model, against the pressure control segment of the TCPE experiment is shown in Fig. 12a-f. The jet velocity in this case was 12 cm/sec and the jet Weber number was 0.71. At this moderate Weber number, the jet only minimally into the ullage. The shape and deformation of the ullage and the penetration depth of the geyser as predicted by the CFD model all agree well with the captured experimental images as evident from a comparison of the CFD predictions in Fig 12e with the experimental image in Fig 12f. Fig 12a also indicates that the predicted evolution of pressure decline in the tank starting at, t= 600 sec, when the jet is started, follows closely the experimental trend.

The final microgravity validations of CFD model are performed against the self-pressurization and pressure control data provided by the Zero Boil-Off Tank experiment that was undertaken in the 2017-2018 timeframe aboard the ISS[25, 46]. As described before the microgravity tests were performed in a small-scale transparent acrylic tank using, Perfluoro-n-Pentane (PnP), as the simulant transparent low boiling point phase change fluid. The validation of the SI-CFD and VOF-CFD models against the ZBOT data was extensive and successful and included more than 30 cases that encompassed self-pressurization, jet ullage interaction, and subcooled jet mixing pressure control case studies[25,35,46.47].

A microgravity self-pressurization validation case is presented in Fig 13 where the tank is heated by the vacuum jacket heating, the tank fill level is 75% and it is subject to an effective gravitation field of $5(10)^{-6}$ g. In this case, the vacuum jacket is uniformly heated to maintain its temperature always 1 degree above the average temperature of the tank wall (see Fig. 13e). Consequently, as is evident from the flow field and the temperature contours in Fig. 13b, the tank is also almost uniformly heated by the heated vacuum jacket through both radiation and conduction heat transfer across a gap that is evacuated and maintained at a vacuum pressure around 0.01 Pa. This situation mimics global heat leaks into an actual storage tank from its Space environment. At this near vacuum pressure, molecular conduction is still an important heat transfer mechanism and of similar magnitude to the radiation heat transfer across the gap.

The numerical simulations were generated by the axisymmetric SI-CFD model using the T-sat approach for calculating the evaporation–condensation mass transfer that occurs at the phase front. The axisymmetric numerical simulations indicate that during vacuum jacket heating, evaporation takes place at the top of the ullage near the hot wall while condensation ensues in the bottom portion of the ullage, where the interface is next to the subcooled liquid. As a result, there is a net flow of vapor from the top of the ullage towards the bottom section of the interface. This mass transfer flow in the ullage drives clockwise vortices in the liquid next to the phase front that isolate the ullage from the weak natural convection vortices in the bottom of the tank which are driven by the residual gravitational acceleration. As the natural convection currents gain strength upon self-pressurization, they can compress the two upper vortices considerably against the ullage. This intricate flow structure is quite weak – as a result the mode of heat transfer through the liquid is dominated by conduction. The hottest part of the ullage is at the top, close to the wall, where evaporation takes place. The coldest section is at the bottom interface where heat is lost to the liquid and condensation ensues. However, the net mass transfer is still evaporative and as a result after an initial delay, the ullage pressure increases, and the self-pressurization rate approaches a constant slope after about six hours of heating as shown in Fig 13e. The axisymmetric model's predictions of tank pressure and of average tank wall temperature evolutions are compared to their experimental counterparts in Fig. 13d and 13e respectively and indicate an excellent

agreement. Comparison between the predicted and measured local temperatures at various RTD location on the tank wall and in the fluid are shown in Figs. 13f-i and again show excellent agreement. These results provided the first successful validation of a CFD model predictions against undisturbed microgravity self-pressurization data in a sealed (zero-boil-off) tank.

Finally, we will focus attention on validation of the CFD models against the ZBOT microgravity subcooled jet mixing tests. In the validation case considered here, comparisons of the predicted and experimental evolution of fluid flow, ullage deformation and movement, and tank pressure drop created by a 10 cm/sec (T_o-1) subcooled jet flow in a 91% filled tank during forced jet mixing pressure control in microgravity is presented. The simulations were performed by our 3D VOF-CFD model using both LES and RANS-SST turbulent submodels and direct comparisons were made with their experimental white light images and particle streak images counterparts captured during unique Particle-Image-Velocimetry (PIV) measurements in microgravity.

The comparison between the predictions of our two-phase VOF-CFD model using the RANS and LES turbulence submodels and their experimental counterparts are presented in Figs 14 and 15. From Fig 14, it becomes evident that by capturing the complex large eddy structure of the turbulent mixing flow with numerical and physical accuracy, the LES VOF-CFD model can predict the influence of the jet on the shape, deformation, and movement of the ullage under microgravity conditions with impressive fidelity. However, the RANSVOF-CFD model, which integrates the detailed effects of the turbulent eddies in favor of faster engineering computations, predicts the settling of the ullage at an incorrect position in the test tank at t = 38.7 s, and misses entirely the correct initial dynamic ullage behavior.

The evolution of the tank pressure during the first 6 minutes of the 10 cm/sec (T_o-1) subcooled jet mixing test is shown in 15a. The experimental results show that in the first 20 s of subcooled jet mixing, the tank pressure goes through an initial rapid drop followed by a more gradual decline. The RANS CFD model does not capture this initial drop, while the LES model predicts it quite well. This is to be expected, since, as shown previously, the RANS model is not able to simulate the ullage deformation and movement with fidelity and predicts a premature settling of the ullage into an incorrect stationary position. However, the long-term pressure drop in the tank (30 mins) occurs when the ullage is hovers around its final position in the middle of the tank as in Fig 14d. Therefore, it is governed more by the net removal of heat from the test cell through the mixing and cooling process rather than by the initial jet impact and ullage deformation and movement. Thus, as shown in Fig 15b, the RANS model provides a good representation of the long-term cooling behavior and pressure decline rate of the ullage. This is good news for practical engineering applications, since, due to the overwhelming computational burden, it is not possible to model the whole long term cooling-depressurization interval with the LES VOF-CFD model.

V. Conclusion

A comprehensive overview of recent model validation case studies of propellant tank pressurization and pressure control was presented. The two main CFD models, namely, SI-CFD and VOF-CFD, that have been validated and discussed were developed through in-house development and customization in the framework of the industry-standard Ansys/Fluent multi-purpose CFD code. A diverse set of 1g and microgravity experiments were selected for validation in order to anchor the models' fidelity across fluid types, gravity environments, and spatial scales. The results are promising and show the established credibility and reliability of the models for engineering predictions and increasing the confidence in the CFD models to be used as effective and reliable computational tools for the design of future propellant tanks for in-orbit or on-surface applications. From a scientific point of view, the CFD models are still lacking in two important areas:

1. Delineating the dissipating influence of the interface on turbulence and its impact on interfacial mass, momentum, and heat transfer during pressurization and pressure control.
2. Correctly predicting the interfacial phase change mass transfer for nonequilibrium situations or dynamic conditions with major interfacial deformations and fragmentation where kinetics may dictate interfacial mass transfer with hard to specify accommodation coefficients. Here, the use of accommodation coefficients as a tuning parameter has so far provided only an engineering solution for the VOF models.

Acknowledgments

Funding and programmatic support from the NASA Space Technology Mission Directorate (STMD) and Microgravity Biological and Physical Sciences (BPS) Division at NASA Headquarters through the ZBOT Experiment science investigations, and the Evolvable Cryogenics and Cryogenic Portfolio Projects at NASA GRC are gratefully acknowledged.

References

1. Salzman, "Fluid management in space-based systems", *Proceedings of the Engineering, Construction, and Operations in Space*, 5th international conference on space, Vol. 1, 1996, p. 521–6.
2. McQuillen J, Rame E, Kassemi M, Singh B, Motil B, "Results of the Workshop on Two-Phase Flow, Fluid Stability and Dynamics: Issues in Power, Propulsion, and Advanced Life Support Systems*". NASA/TM-2003-212598* (2003)
3. Kassemi M, Kartuzova O, Hylton S, "Validation of Two-Phase CFD Models for Propellant Tank Self-Pressurization: Crossing Fluid Types, Scales, and Gravity Levels", *Cryogenics* Vol. 89 pp. 1–15, Jan 2018.
4. Kassemi M, Kartuzova O, "Effect of Interfacial Turbulence and Accommodation Coefficient On CFD Predictions of Pressurization and Pressure Control in Cryogenic Storage Tank", *Cryogenics*, Vol. 74, pp.138-153, 2016.
5. Barsi S, Kassemi M, "Numerical and Experimental Comparisons of the Self-Pressurization Behavior of an LH2 Tank in Normal Gravity", *Cryogenics*, 48(3/4), pp. 122-129, 2007.
6. Hasan, M., Lin, C., and Dresar, N. V., "Self-pressurization of a flight-weight liquid hydrogen storage tank subjected to low heat flux", *NASA TM 103804*, 1991
7. Van Dresar, N., Lin, C., and Hasan, "Self-pressurization of a flight-weight liquid hydrogen tank: Effects of fill level at low wall heat flux", *NASA TM 105411*, 1992.
8. Ward, W.D., et al, "Evaluation of AS-203 Low-Gravity Orbital Experiment", *NASA CR 94045* (Chrysler Corp. Space Div. Technical Report BB-3.4.3-5-101), 13 January 1967.
9. Lacovic, R., Yeh, F., S.V. Szabo, J., Brun, R., Stofan, A., and Berns, J., "Management of cryogenic propellants in a full-scale orbiting space vehicle", *NASA TN D-4571*, 1968.
10. Aydelott, J.C. "Axial Jet Mixing of Ethanol in Cylindrical Containers During Weightlessness," *NASA TP-1487*, 1979.
11. Hasan, M.M., and Lin, C.S., "Axisymmetric confined turbulent jet directed towards the liquid surface from below," *NASA TM 101409*, 1989.
12. Lin, C.S., and Hasan, M.M., "Effect of Liquid Surface Turbulent Motion on the Vapor Condensation in a Mixing Tank," *Transport Phenomena in Heat and Mass Transfer*. Elsevier, pp. 1526–1537, 1992
13. Kartuzova, O., Kassemi, M., "Modeling Active Pressure Control in a Large-Scale Cryogenic Storage Tank in Normal Gravity," *AIAA 2012-3983*, Proceedings of the 48th AIAA/ASME/SAE/ASEE Joint Propulsion Conference, Atlanta, GA, 2012
14. Hastings, L.J., Flachbart, R.H., Martin, J.J., Hedayat, A., Fazah, M., Lak, T., Nguyen, H., Bailey J.W., 'Spray Bar Zero-Gravity Vent System for On-Orbit Liquid Hydrogen Storage", *NASA TM-212926*, 2003.
15. Kartuzova O, and Kassemi M, "CFD Modeling of the Multipurpose Hydrogen Test Bed (MHTB) Self-Pressurization and Spray Bar Mixing Experiments in Normal Gravity: Effect of the Accommodation Coefficient on the Tank Pressure", *AIAA 2015-3769*, 51st AIAA/ASME/SAE/ASEE Joint Propulsion Conference, Orlando, Florida, 27-29, July 2015.
16. Kartuzova O, Kassemi M, "Modeling K-Site LH2 Tank Chilldown and no Vent Fill in Normal Gravity", *AIAA-2017-4662*, Proceedings of the 53rd AIAA/SAE/ASEE Joint Propulsion, Atlanta, Georgia, 10–12, July 2017.
17. T. Page "Thermal Test Report and Thermal Math Model Test Correlation Report for the Cryogenic Propellant Storage and Transfer (CPST) Engineering Development Unit (EDU)" *NASA Report EV34-19-002*, NASA Marshall Space Flight Center, August 2019
18. Kartuzova O, Kassemi M, Hauser D, "Modeling Autogenous Pressurization and Draining of a Cryogenic Storage Tank in Normal Gravity", SciTech Forum, National Harbor, MD, January 2023.
19. Himeno T, Sugimori D, Uzawa T, Watanabe KT, Nonaka S, "Heat Exchange and Pressure Drop Enhanced by Violent Sloshing", *AIAA-2010-6979*, Proceedings of the 46th AIAA/ASME/SAE/ASEE Joint Propulsion Conference and Exhibit, Nashville, TN, USA, 2010.
20. Himeno T, et al., "Investigation on Phase Change and Pressure Drop Enhanced by Violent Sloshing of Cryogenic Fluid", *AIAA 2018-4755*, AIAA Propulsion and Energy Forum, July 2018, Cincinnati, OH, 2018.
21. Kartuzova O, Kassemi M, "A Computational Study of the Effect of Sloshing with High Level of Lateral Acceleration on the Heat Transfer and Pressure Drop in a Small-Scale Tank in Normal Gravity", *FEDSM-2018-83113*, The 2018 ASME FEDS Meeting, Montreal, Canada, July 2018.
22. Kartuzova, O, Kassemi, M, Umemura, Y, Kinefuchi, K, Himeno, T, "CFD Modeling of Phase Change and Pressure Drop during Violent Sloshing of Cryogenic Fluid in a Small-Scale Tank", *AIAA 2020-3794*, AIAA Propulsion and Energy 2020 Forum, New Orleans, August 24-28, 2020
23. Barsi S. and Kassemi, M. "Investigation of Tank Pressurization and Pressure Control-Part I: Experimental Study", *ASME Journal of Thermal Science & Engineering Applications*, Vol. 5, No 2, pp- 041005: 1-20, December 2013.
24. Barsi S. and Kassemi, M. "Investigation of Tank Pressurization and Pressure Control-Part II: Numerical Modelling", ASME *Journal of Thermal Science & Engineering Applications*, Vol. 5, No 2, pp- 041006: 1-9, December 2013.
25. Kassemi M, Kartuzova O, Hylton S, "Zero-Boil-Off Tank Experiment - 1G and Microgravity Pressurization & Pressure Control Results", *Paper IAC-18-A2.2.6-43028*, The 65th International Astronautical Congress (IAC), Bremen, Germany, Oct 2018.
26. Johnson, W.L, Balasubramaniam, R., Hibbs, R.G., Zimmerli, G.A., Asipauskas, M., Bittinge, S.A., Dardano, C., and Koci, F.D., "Demonstration of Multilayer Insulation, Vapor Cooling of Structure, and Mass Gauging for Large-Scale Upper Stages: Structural Heat Intercept, Insulation, and Vibration Evaluation Rig (SHIIVER) Final Report", *NASA/TP-20205008233*, August 2021.

27. Lemmon, E.W., McLinden, M.O., and Friend, D.G., "Thermophysical Properties of Fluid Systems, in NIST Chemistry WebBook", *NIST Standard Reference Database Number 69*, Eds. Linstrom, P.J., and Mallard, W.G., National Institute of Standards and Technology, Gaithersburg MD, 20899, http://webbook.nist.gov.
28. Schrage, R.W., "*A theoretical study of interphase mass transfer"*, Columbia University Press, New York, 1953
29. Hirt, C.W., and Nichols B.D., "Volume of fluid (VOF) method for the dynamics of free boundaries", *Journal of Computational Physics*, Vol. 39 No. 1, 1981, pp. 201-225.
30. Brackbill J.U., Kothe, D.B., Zemach, C., "A continuum method for modeling surface tension", *J. Comp. Phys.*, Vol. 100, 1992, pp. 335–354
31. O. Kartuzova and M. Kassemi, "Modeling Droplet Heat and Mass transfer during Spray Bar Mixing of the Multipurpose Hydrogen Test Bed (MHTB) Tank in Normal Gravity", *AIAA2016-4673*, Proceedings of the 52nd AIAA/ASME/SAE/ASEE Joint Propulsion Conference, Salt Lake City, Utah, 25-27 July 2016.
32. Ranz, W. E. and Marshall, W. R., Jr. "Evaporation from Drops, Part I," *Chemical Engineering Progress*, Vol. 48, No. 3, 1952, pp. 141–146.
33. Ranz, W. E. and Marshall, W. R., Jr. "Evaporation from Drops, Part II," *Chemical Engineering Progress*, Vol. 48, No. 4, 1952, pp. 173–180.
34. Kartuzova, O., Kassemi, M., Hauser, D., "CFD Model Development of a Cryogenic Storage Tank Self-Pressurization in Normal Gravity and Validation against SHIIVER Experiment", *2022 AIAA SciTech Forum*, National Harbor, MD, January 2023.
35. Kassemi, M., Hylton, S., and Kartuzova, O. "Zero-Boil-Off Tank (ZBOT) Experiment – CFD Self-Pressurization Model Validation with Ground-Based & Microgravity Results," *AIAA2018-2940*, Proceedings of the 54th AIAA/SAE/ASEE Joint Propulsion Conference, Cincinnati, OH, July 2018.
36. Kartuzova, O., Kassemi, M., Agui, J., Moder, J., "A CFD model for the Multipurpose Hydrogen Test Bed (MHTB) Ground-Based Self-Pressurization and Pressure Control Experiments," Proceedings of the 11th AIAA/ASME Joint Thermophysics and Heat Transfer Conference, *AIAA 2014-3361*, Atlanta, GA, 2014.
37. Kartuzova, O., Kassemi, M., Agui, J., Moder, J., "Self-Pressurization and Spray Cooling Simulations of the Multipurpose Hydrogen Test Bed (MHTB) Ground-Based Experiment," Proceedings of the 50th AIAA/ASME/SAE/ASEE Joint Propulsion Conference, *AIAA 2014-3578*, Cleveland, OH, 2014.
38. Ward, W.D., et al, "Evaluation of AS-203 Low-Gravity Orbital Experiment", NASA CR 94045 (Chrysler Corp. Space Div. Technical Report BB-3.4.3-5-101), 13 January 1967.
39. Lacovic, R., Yeh, F., S.V. Szabo, J., Brun, R., Stofan, A., and Berns, J., "Management of cryogenic propellants in a full-scale orbiting space vehicle", *NASA TN D-4571*, 1966.
40. Kartuzova, O., Kassemi M, "Modeling Interfacial Turbulent Heat Transfer during Ventless Pressurization of a Large-Scale Cryogenic Storage Tank in Microgravity", *AIAA 47th Joint Propulsion Conference*, San Diego, CA, 2011.
41. Grayson, G., Lopez, A., Chandler, F., Hastings, L., and Tucker, S, "Cryogenic tank modeling for the Saturn AS-203 experiment". *AIAA 2006-5258*, 2006.
42. Bentz, M.D. "Tank Pressure Control in Low Gravity by Jet Mixing," *NASA-CR-191012*, March 1993.
43. Hasan, M.M., Lin, C.S., Knoll, R.H., and Bentz, M.D. "Tank Pressure Control Experiment: Thermal Phenomena in Microgravity," *NASA Technical Paper – 3564*, March 1996. https://ntrs.nasa.gov/citations/19960017263
44. O. Kartuzova and M. Kassemi, "Modeling Ullage Dynamics of Tank Pressure Control via Jet Mixing in Microgravity", *Paper AIAA 2016-4677*, Proceedings of the 52nd AIAA/ASME/SAE/ASEE Joint Propulsion Conference, Salt Lake City, Utah, 25-27 July 2016.
45. O. Kartuzova and M. Kassemi, "CFD Prediction of Microgravity Self-Pressurization and Pressure Control and Validation against a Tank Pressure Control Experimen"t, *AIAA-2017-4662*, Proceedings of the 53rd Joint Propulsion, Atlanta, Georgia, 10–12 July 2017.
46. Kassemi M, Hylton S, Kartuzova O, "Results of Microgravity Zero-Boil-Off Tank (ZBOT) Experiment & CFD Model Validation", *Paper Elgra-2019-072*, 26th European Low Gravity Research Association Biennial Symposium and General Assembly and the 14th International Conference on "Two-Phase Systems for Space and Ground Applications", European Space Agency Topical Teams meetings, Granada, Spain, September 24-27, 2019
47. Kartuzova O, Kassemi M, "CFD Jet Mixing Model Validation against Zero-Boil-Off Tank (ZBOT) Microgravity Experiment", *AIAA 2019-4282***,** 55th AIAA/ASME/SAE/ASEE Joint Propulsion Conference, Indianapolis, IN, 19-22 August 2019.

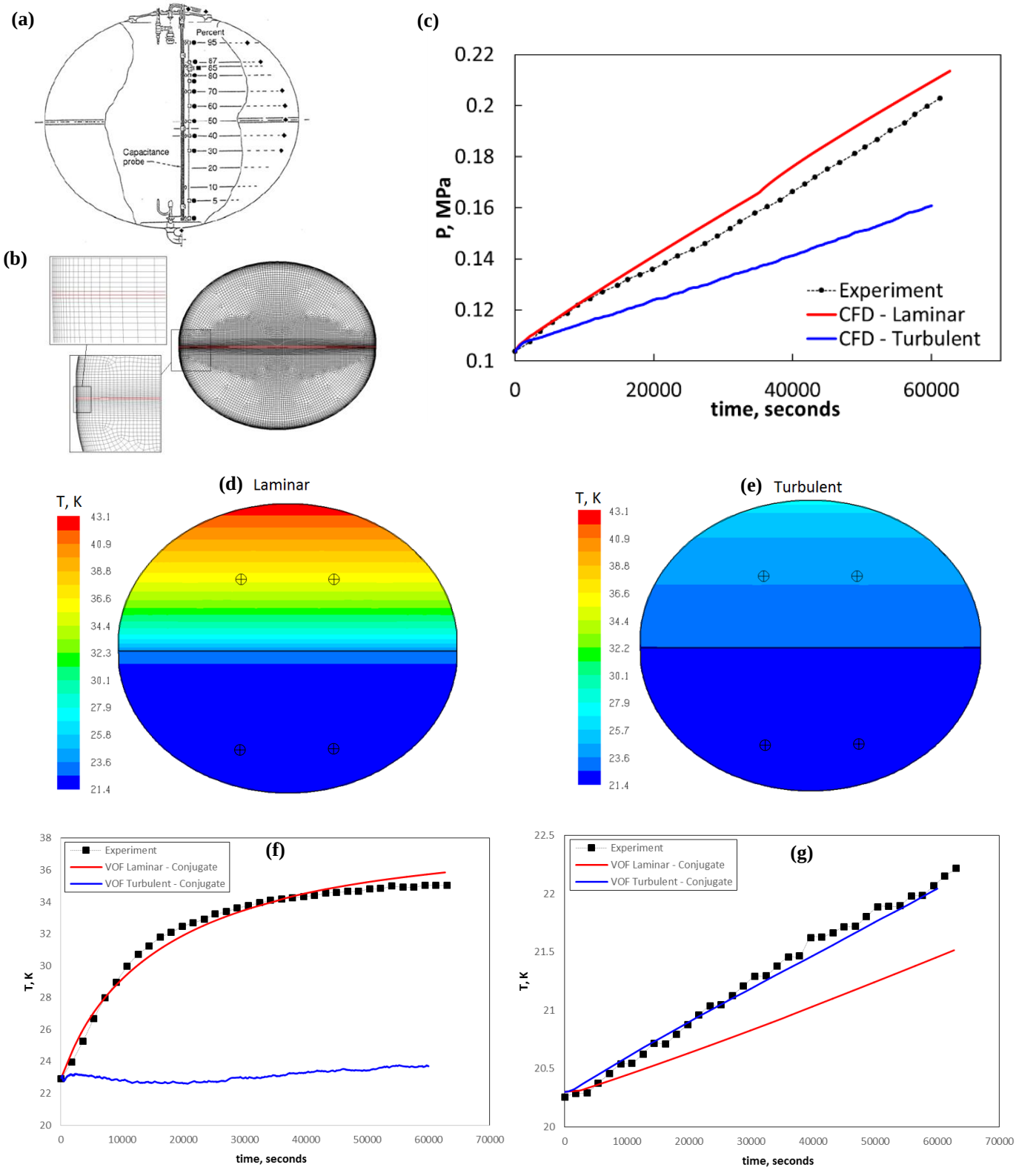


Figure 1: Comparison of laminar and turbulent conjugated VOF models' predictions of LH2 propellent tank self-pressurization against experimental results for the 50% filled K-site tank subject to a uniform heat flux of 3.5 W/m^2: (a) Schematic of K-site Tank; (b) Computational Grid; (c) Tank pressure evolution (d) laminar temperature field at the end of self-pressurization; (e) turbulent temperature field at the end of self-pressurization; (f) predicted and measured evolution of temperature at point in the vapor: and (g) predicted and measured evolution of temperature at a point in the liquid. The location of the temperature measurements in (f) and (g) are indicated by circles in (d) and (e).

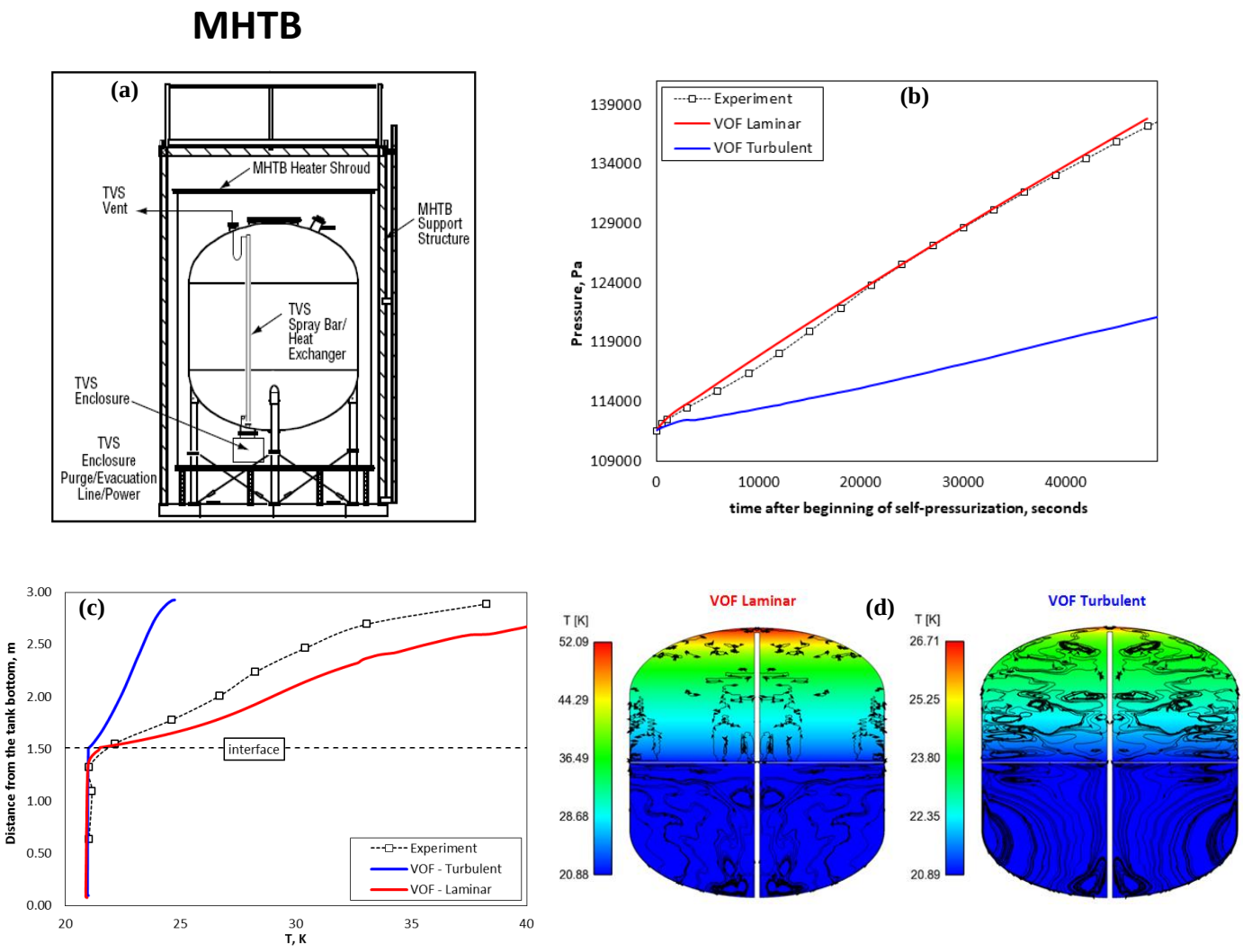


Figure 2: Comparison of laminar and turbulent conjugated and non-conjugated VOF models' predictions of LH2 propellant tank self-pressurization against experimental results for the 50% filled MHTB tank subject to a nonuniform heat flux of 0.90 W/m^2 imposed on the un-wetted section and 2.08 W/m^2 on the wetted surface: (a) Schematic of MHTB Tank; (b) Tank pressure evolution; (c) predicted and measured temperature distribution in the tank; (d) laminar and turbulent temperature fields at the end of self-pressurization.

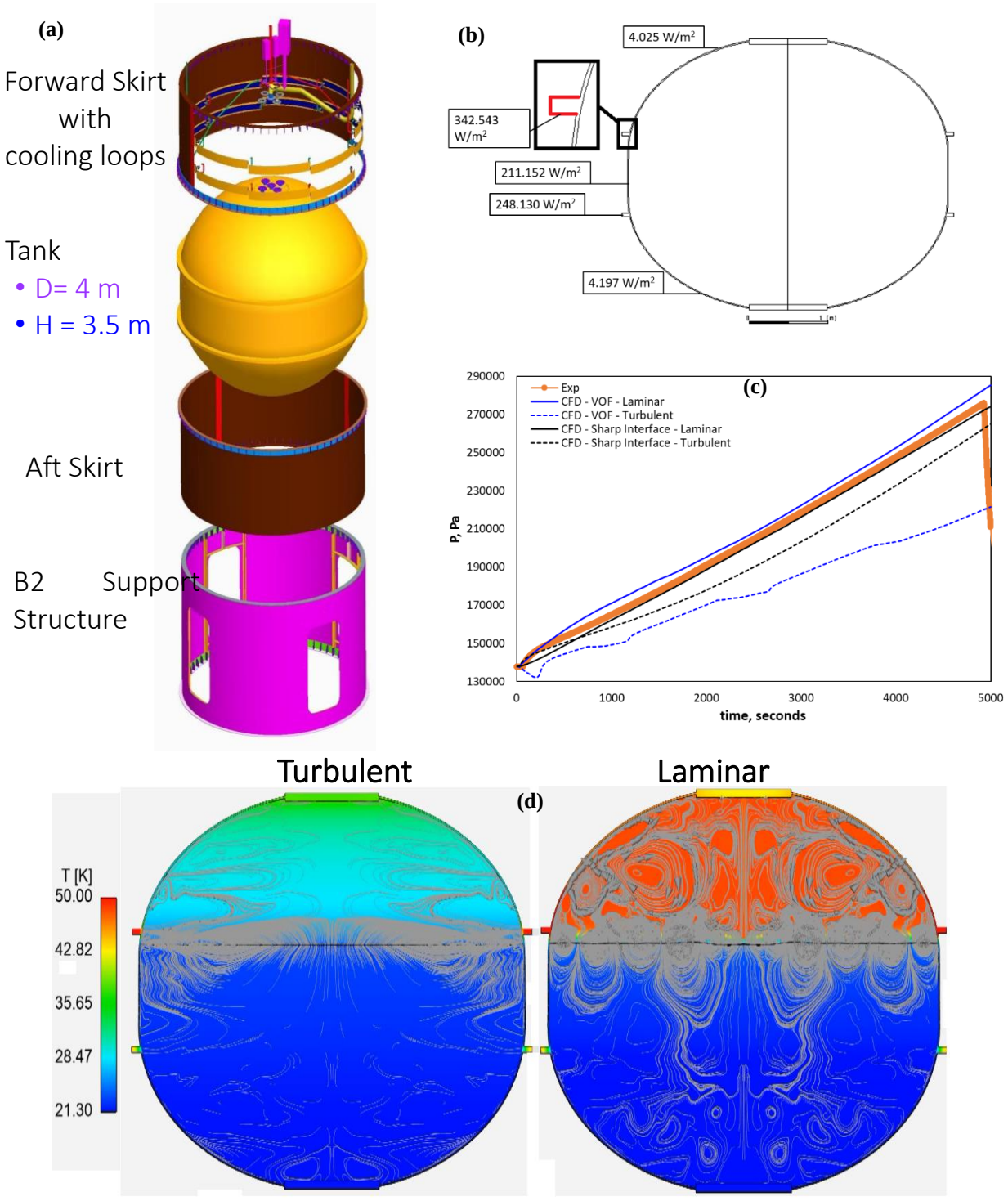


Figure 3: Comparison of laminar and turbulent conjugated SI-CFD and VOF-CFD models' predictions of propellant tank self-pressurization against experimental results for SHIIVER tank with an initial fill level of 67.36% and subject to a nonuniform heat flux: (a) Schematic of SHIIVER Tank; (b) Nonuniform tank heat load distribution; (c) predicted and measured evolution of pressure in in the vapor; (d) laminar and turbulent temperature fields predicted by the VOF-CFD model at the end of self-pressurization.

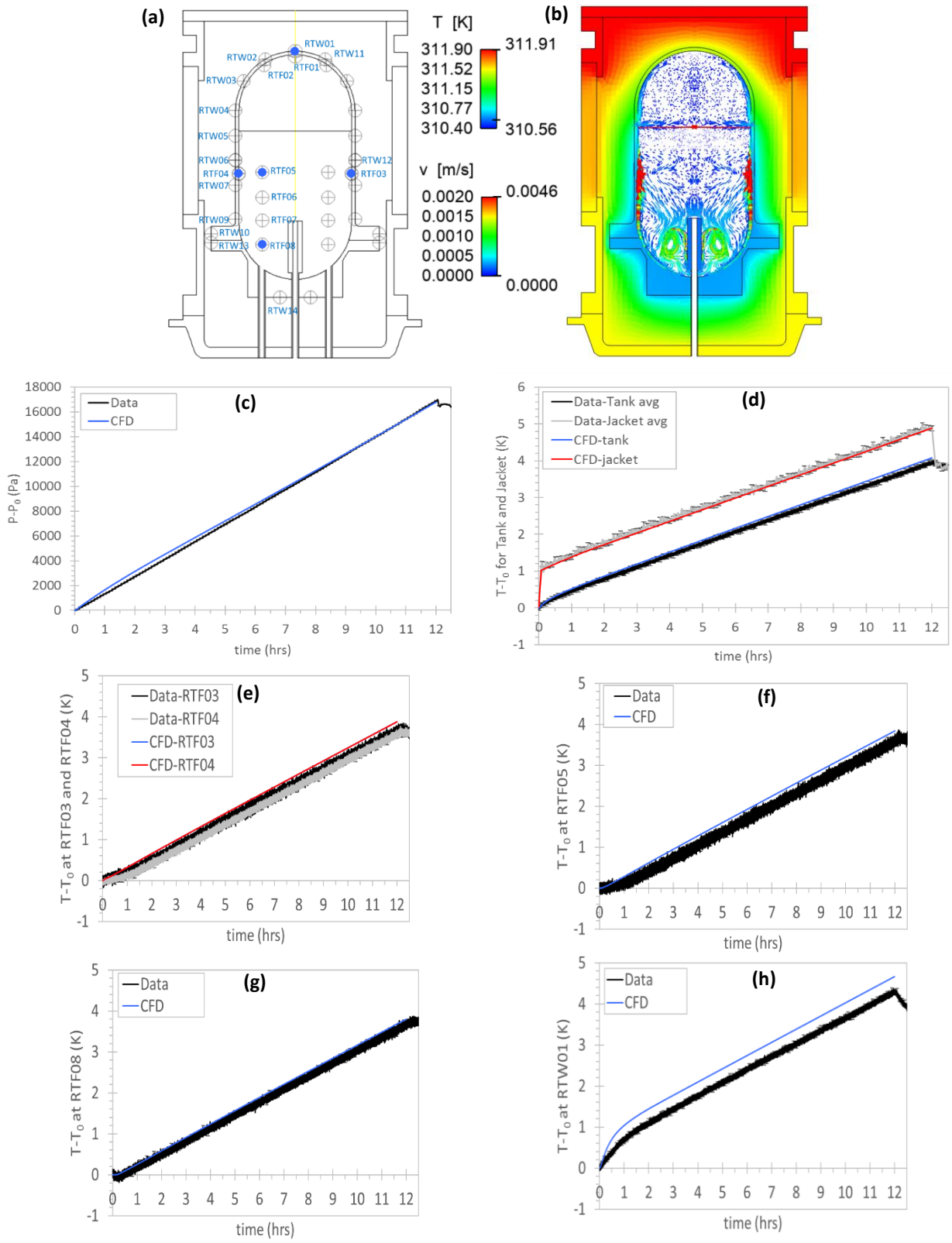


Figure 4: Validation of SI-CFD model against ground-based ZBOT self-pressurization experiments for a vacuum jacket heating mode with $T_j = T_w + 1$ K and a PnP fill level of 70%: (a) Schematic of ZBOT tank showing the location of wall and fluid temperature sensors; (b) Predicted flow and temperature fields in 1g; (c) comparison between predicted and measured evolution of tank pressure; (d) Comparison of area average test tank wall temperature evolution against the measured value; (e-h) comparison predicted local fluid and tank wall temperatures against their experimental counterparts at various RTD sensor locations on the tank.

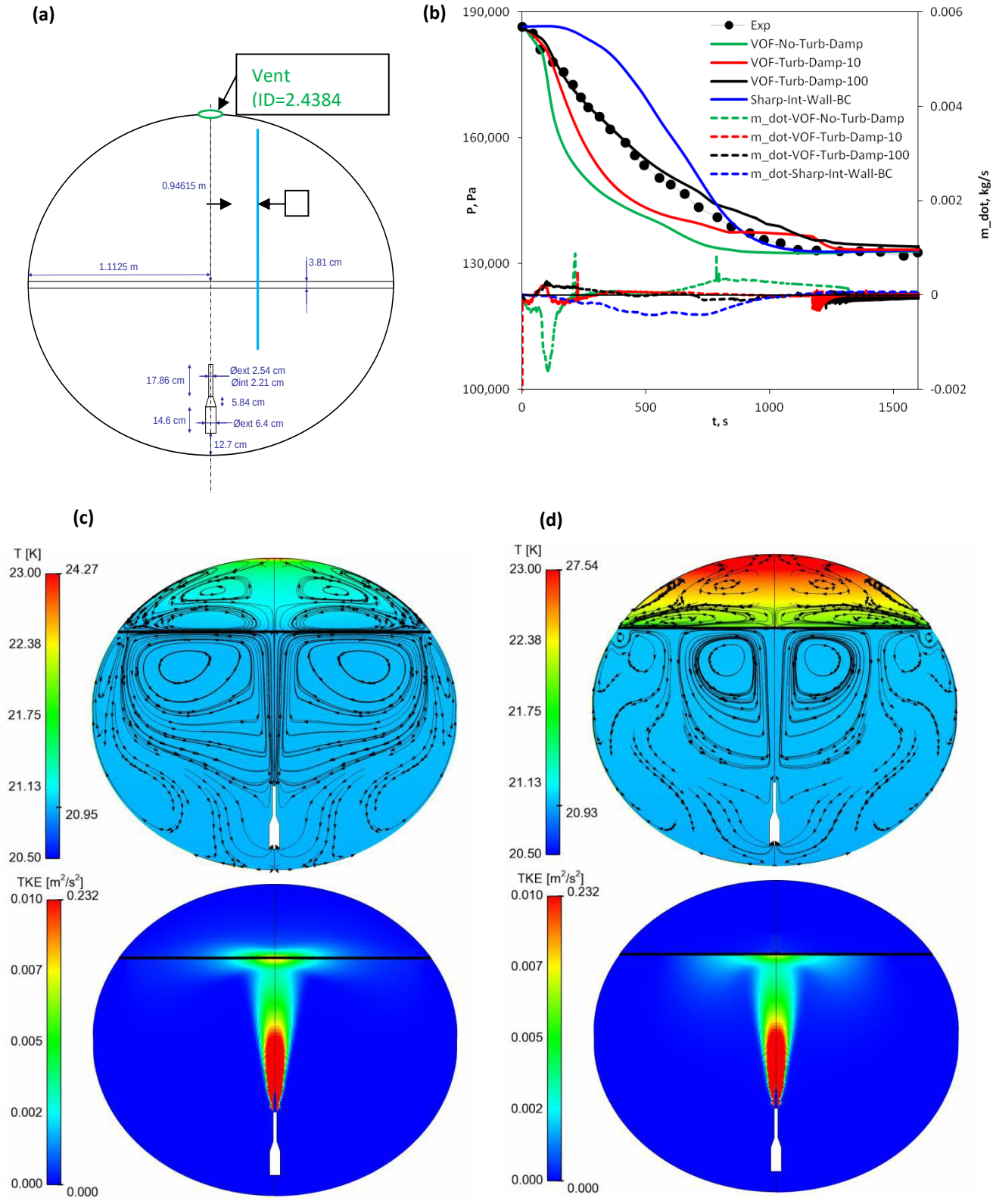


Figure 5: Validation comparison for Ksite LH2 jet mixing case 436 (86% fill ratio; Re_{jet} = 160,000) at t= 120sec after initiation of mixing: (a) K-site tank schematic; (b) predicted and measured evolution of pressure in the tank with various levels of turbulence damping; (c) VOF-CFD predictions of flow, temperature, and turbulent kinetic energy fields without turbulence damping; (d) VOF-CFD predictions of flow, temperature, and turbulent kinetic energy fields with a turbulence damping of 100.

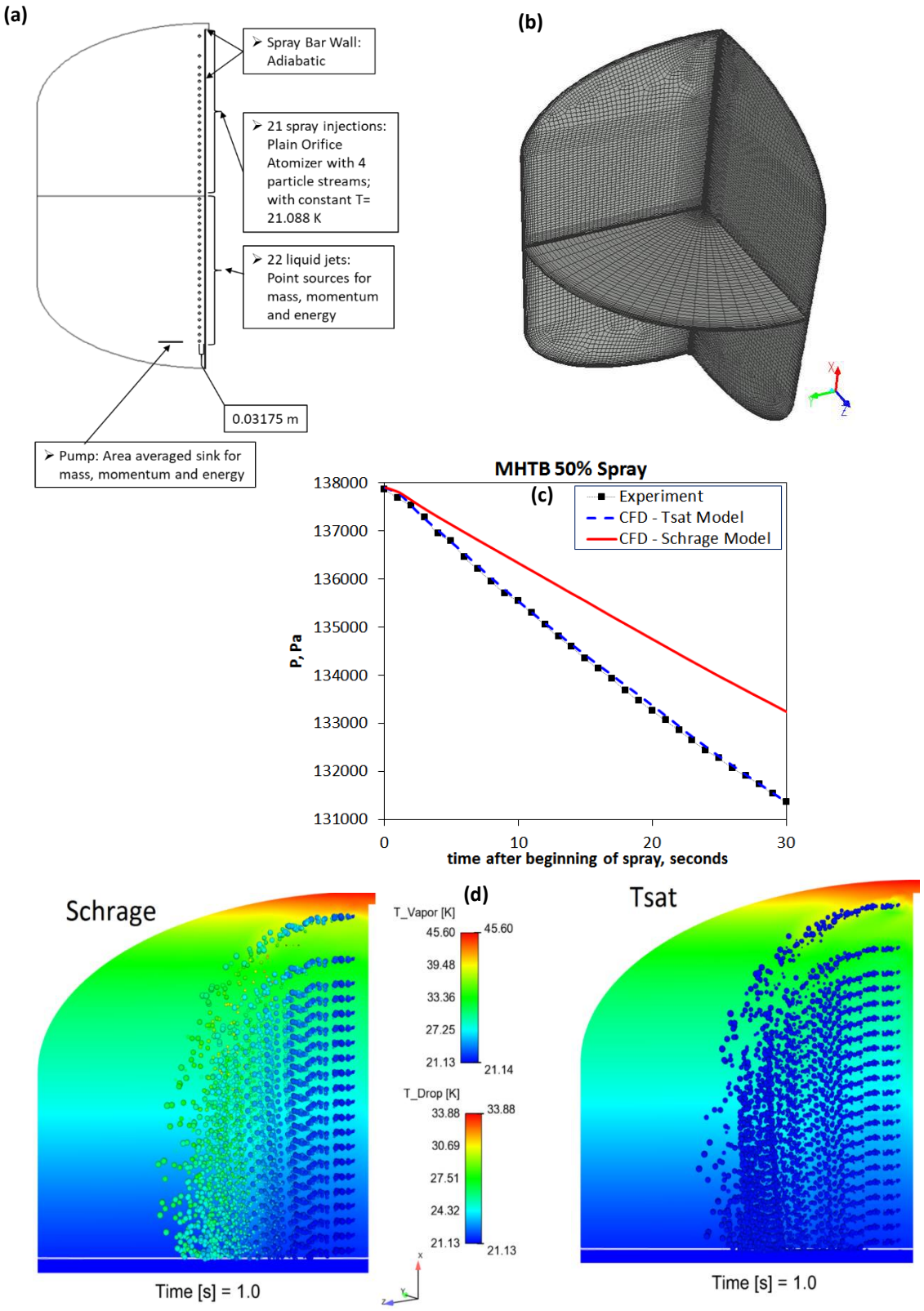


Figure 6: Comparison of VOF-CFD models' predictions of pressure reduction in the MHTB LH2 storage tank against experimental results using the Tsat and Schrage droplet heat transfer and phase change submodels for a fill level of 50%: (a) Schematic of MHTB Tank with the spray-bar; (b) 3D computational grid; (c) Comparison of pressure reduction predictions of VOF-CFD with Tsat and Schrage droplet phase change submodels against MHTB pressure control data; (d) Whole field ullage and droplet temperatures predicted by the VOF-CFD with Tsat and Schrage droplet phase change submodels.

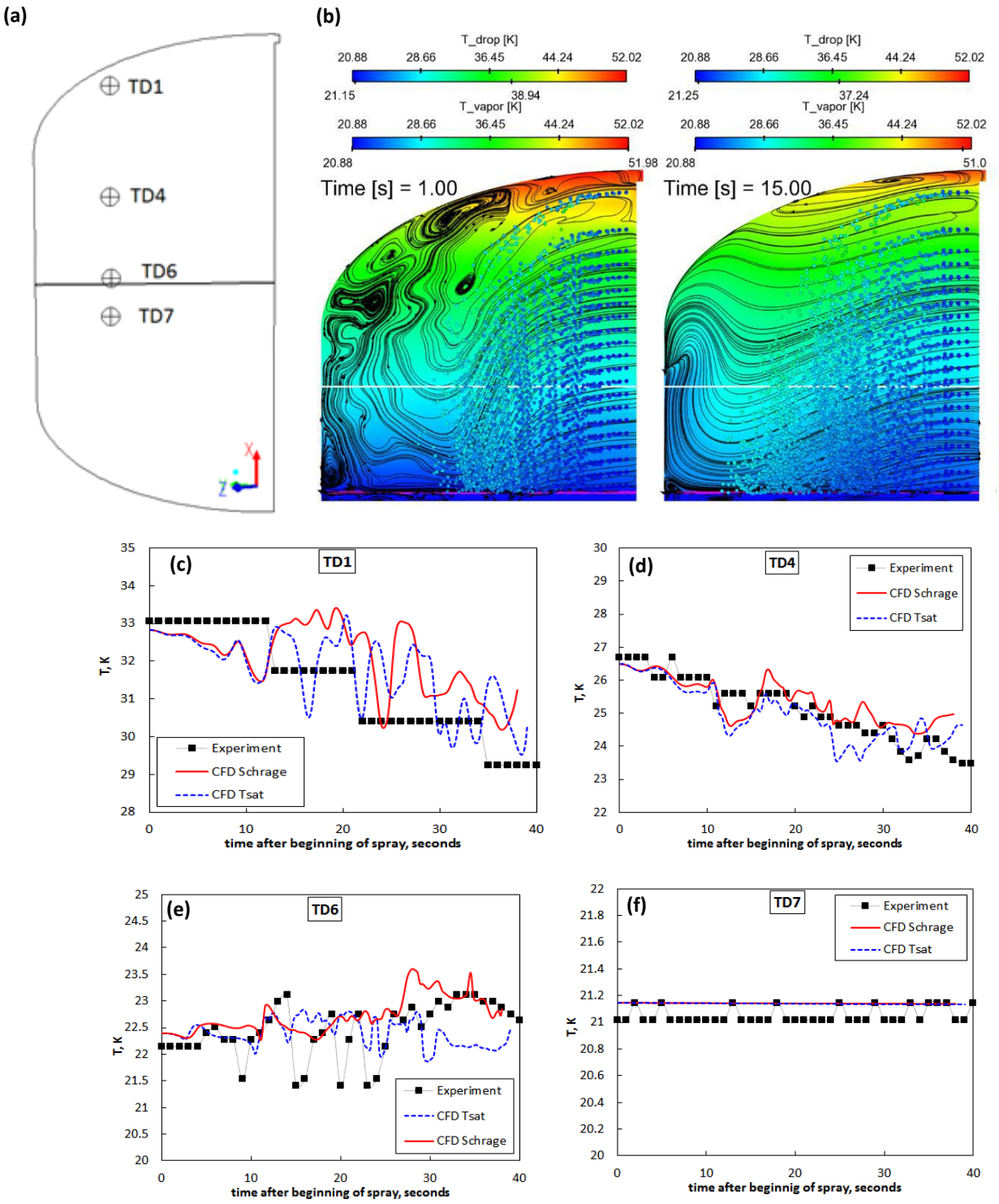


Figure 7: Comparison of VOF-CFD models' predictions of local temperatures in the MHTB LH2 storage tank against experimental results using the Tsat and Schrage droplet heat transfer and phase change submodels for a fill level of 50%: (a) Schematic of MHTB Tank with temperature sensor locations; (b) The whole field ullage and droplet temperatures and the flow field predicted by the VOF-CFD with Schrage droplet phase change submodel at t = 1 sec and t = 15 sec: (c-f) Comparison of temperature predictions at different RTD locations by VOF-CFD model with Tsat and Schrage droplet phase change submodels against MHTB temperature sensor data.

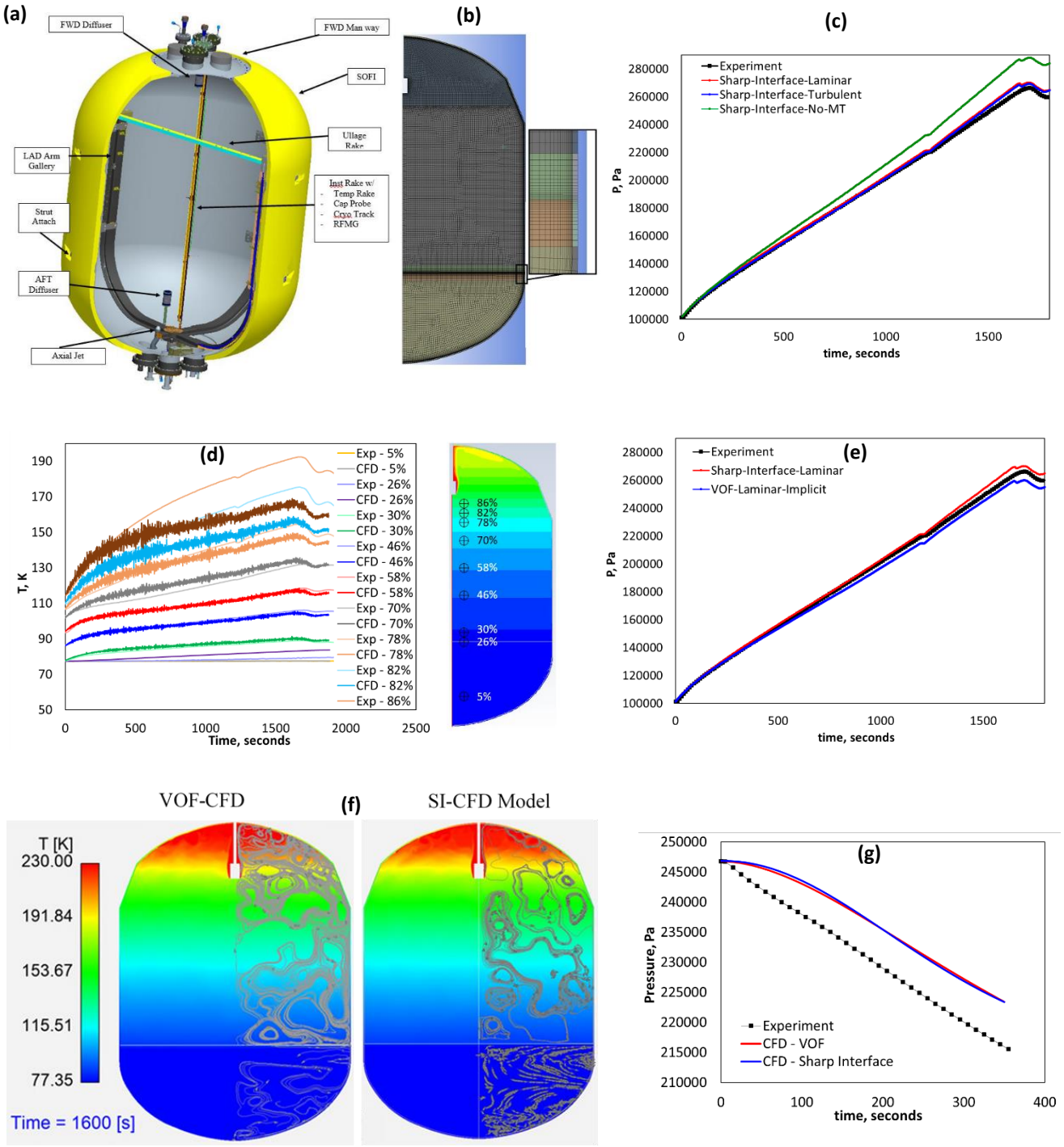


Figure 8: Validation of conjugated turbulent and laminar SI-CFD and VOF-CFD autogenous tank pressurization models against 1g EDU LN2 tank pressurization experiment with a fill level of 26% at uniform initial conditions with T_initial = 77.35 K and P_initial = 101270 Pa: (a) EDU tank schematic; (b) Axisymmetric computational grid; (c) Comparison of pressure predictions of the turbulent and laminar SI-CFD model with and without interfacial mass transfer against EDU experimental tank pressure evolution; (d) Comparison of temperature at various vertical sensor locations by the laminar SI-CFD model against EDU temperature sensor measurements; (e) Comparison of pressure predictions of the laminar SI-CFD and VOF-CFD models against EDU experimental tank pressure evolution: (f) autogeneous pressurization temperature and flow fields predictions by the VOF-CFD and SI-CFD models at t = 1600 sec: (g) Comparison between pressure drop predictions of SI-CFD and VOF-CFD during liquid extraction against their experimental counterpart.

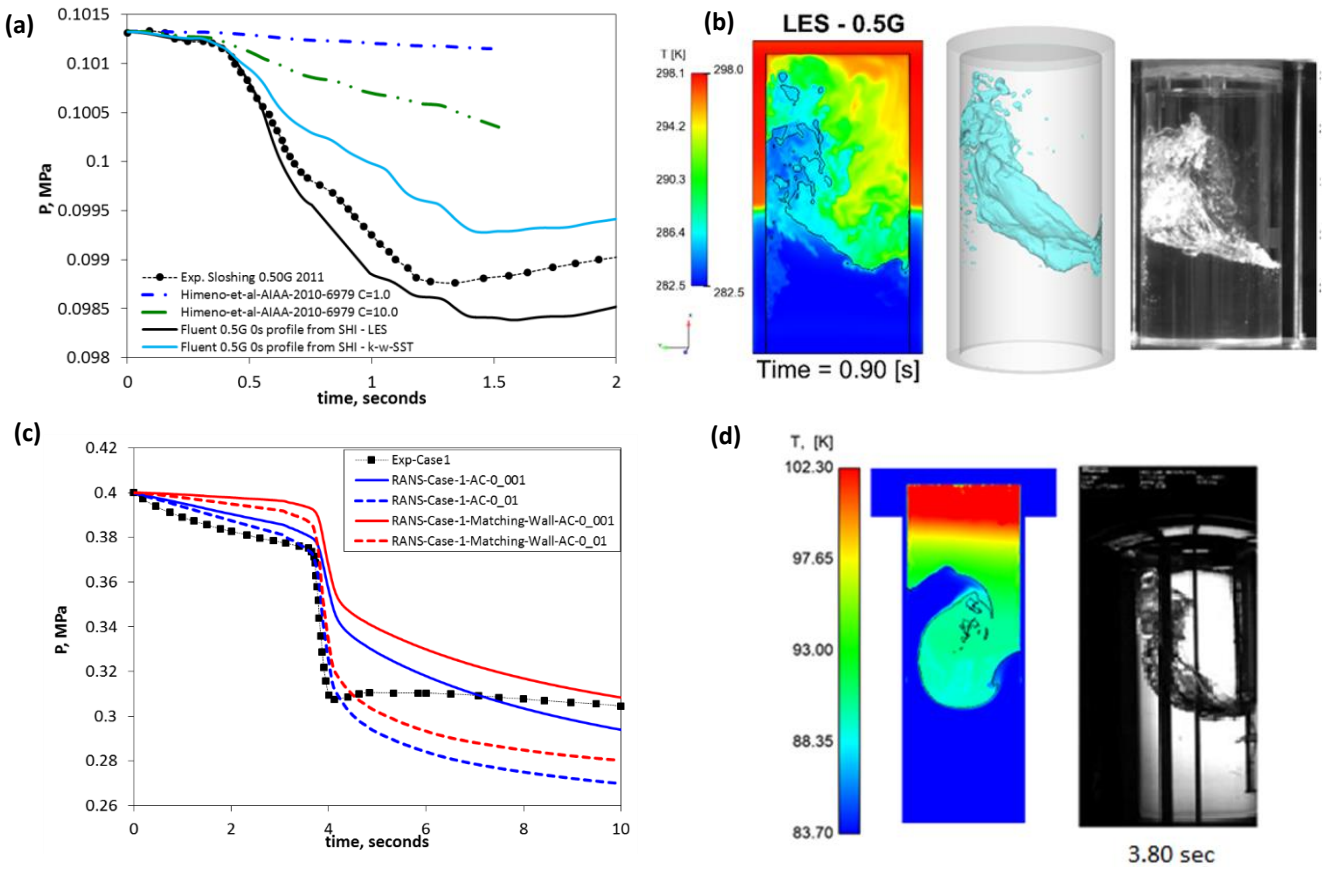


Figure 9: Pressure evolution in the tank during 1g sloshing: (a) Comparison between VOF-CFD predictions and experimental results reported by Himeno et al.[19] for Silicone oil slosh without phase change with a lateral acceleration of 0.5 G. The results of the LES model are compared with the experimental image at 0.9s. (b) Effect of accommodation coefficient – "cold" vs. "matching" wall initial conditions against experimental results by Himeno et al[20] for LN2 slosh with phase change. The results of the LES model are compared with the experimental image at 3.8 s.

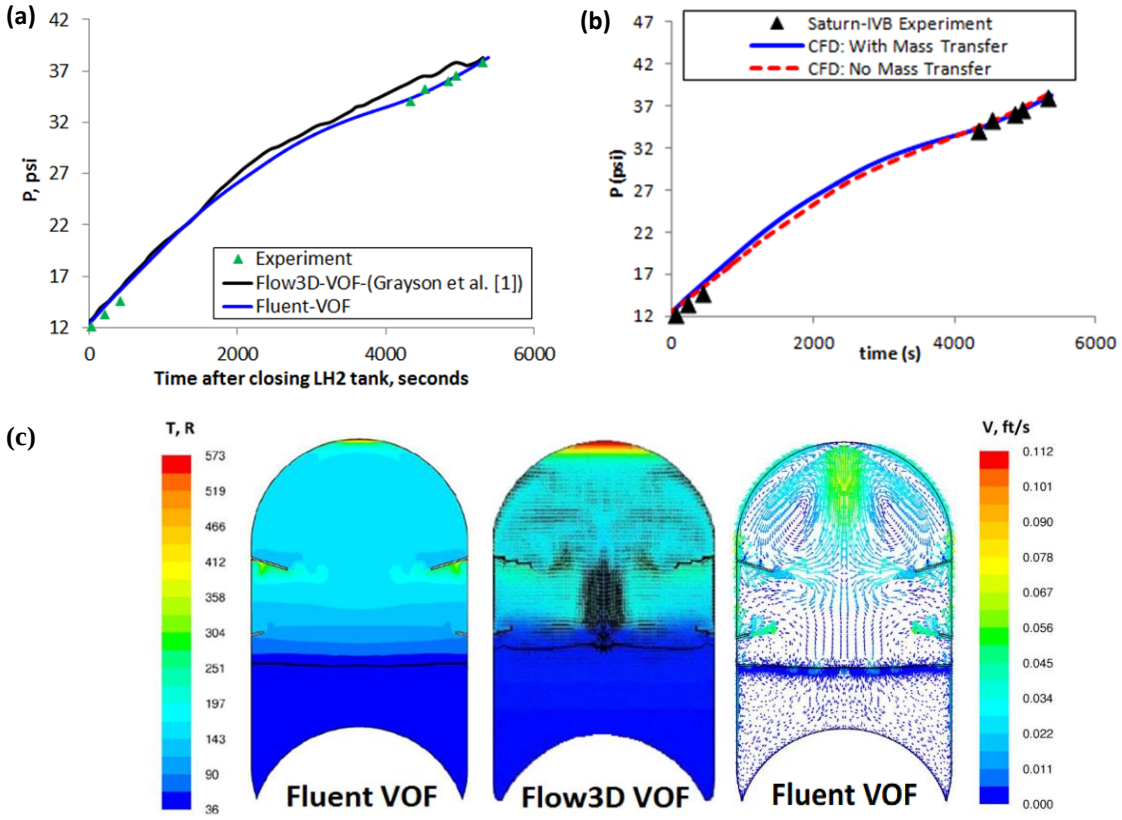


Figure 10: Pressure evolution in the Saturn S-IVB AS-203 LH2 self-pressurization experiment in reduced gravity: (a) Comparison between the Fluent VOF-CFD predictions with Flow3D predictions (Grayson et al[41]) and experimental results: (b) VOF-CFD Self-Pressurization predictions with and without interfacial mass transfer compared to the experimental pressure data; (c) The Fluent VOF-CFD flow and temperature predictions in the tank compared to Flow3D predictions of Grayson et al.[41].

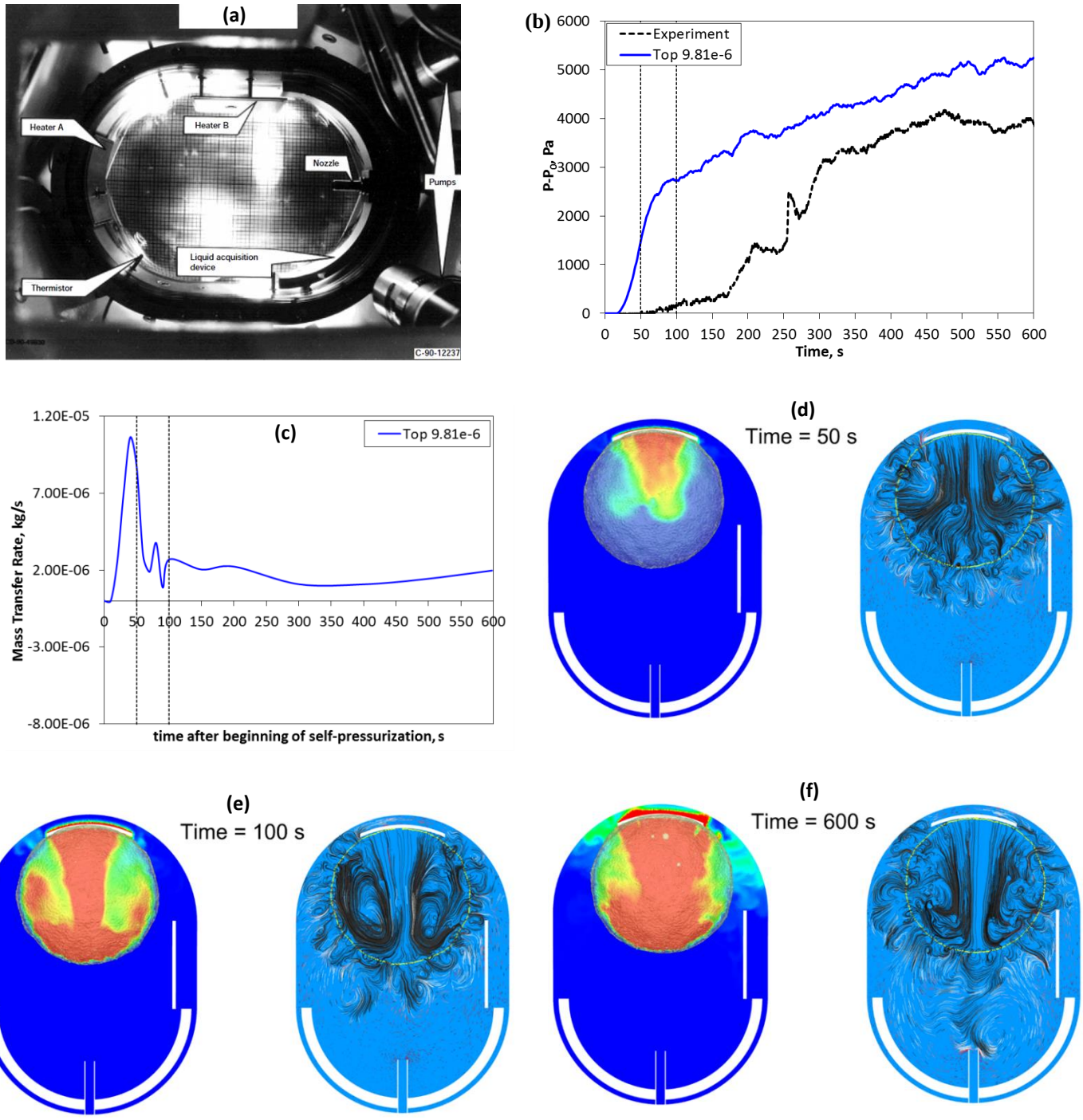


Figure 11: Self Pressurization of the TPCE tank in microgravity: (a) Schematic of the TPCE Test Cell; (b) Comparison of pressure evolution between VOF-CFD predictions and TPCE experimental results; (c) Predicted evolution of evaporative interfacial mass transfer during the self-pressurization test; (d-f) Predicted self-pressurization temperature and velocity fields at t = 50 sec, t = 100 sec, and t = 600 sec respectively.

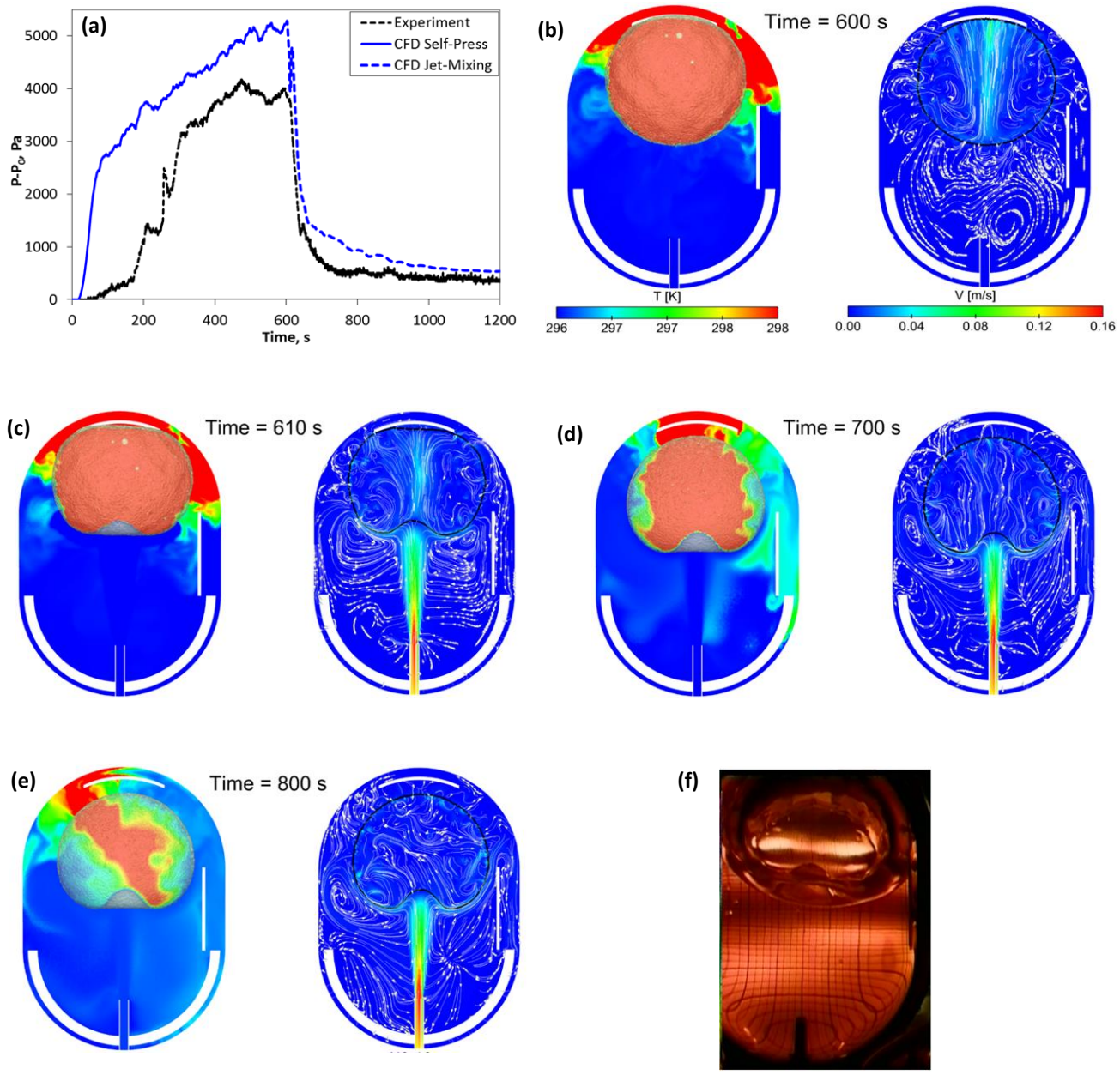


Figure 12: Jet mixing pressure control of the TPCE tank in microgravity: (a) Comparison of pressure evolution between VOF-CFD predictions and TPCE experimental results during jet mixing initiated at t = 600 sec; (b-e) Predicted temperature and velocity fields during jet mixing at t = 600 sec, t = 610 sec, t = 700 sec, and t = 800 sec, respectively; (f) Experimental image of ullage shape and geyser penetration at t= 800 sec.

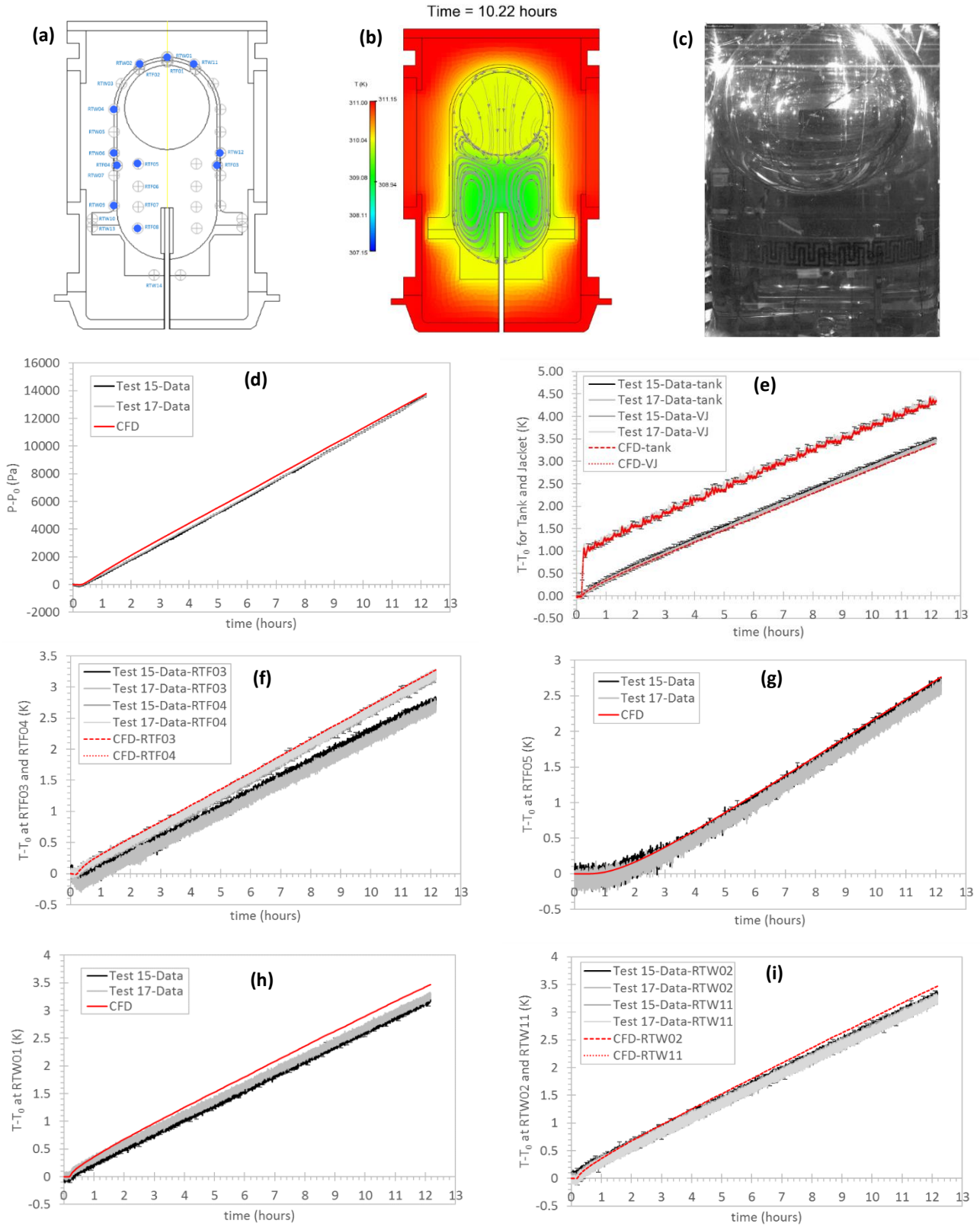


Figure 13: ZBOT vacuum jacket self-pressurization validation for a PnP fill level of 78% and $T_J = T_w+1$ K: (a) Schematic of ZBOT tank indicating the location of temperature sensors; (b) SI-CFD axisymmetric prediction of flow and temperature fields; (c) Experimental image capture showing the shape and position of the ullage during the microgravity self-pressurization test; (d) comparison between SI-CFD prediction of pressure evolution in the tank and its experimental counterpart; (e) Comparison between the area average test tank wall temperature and the measured value; (f-i) comparison of predicted fluid and tank wall temperatures against their experimental counterparts at various RTD sensor locations on the tank.

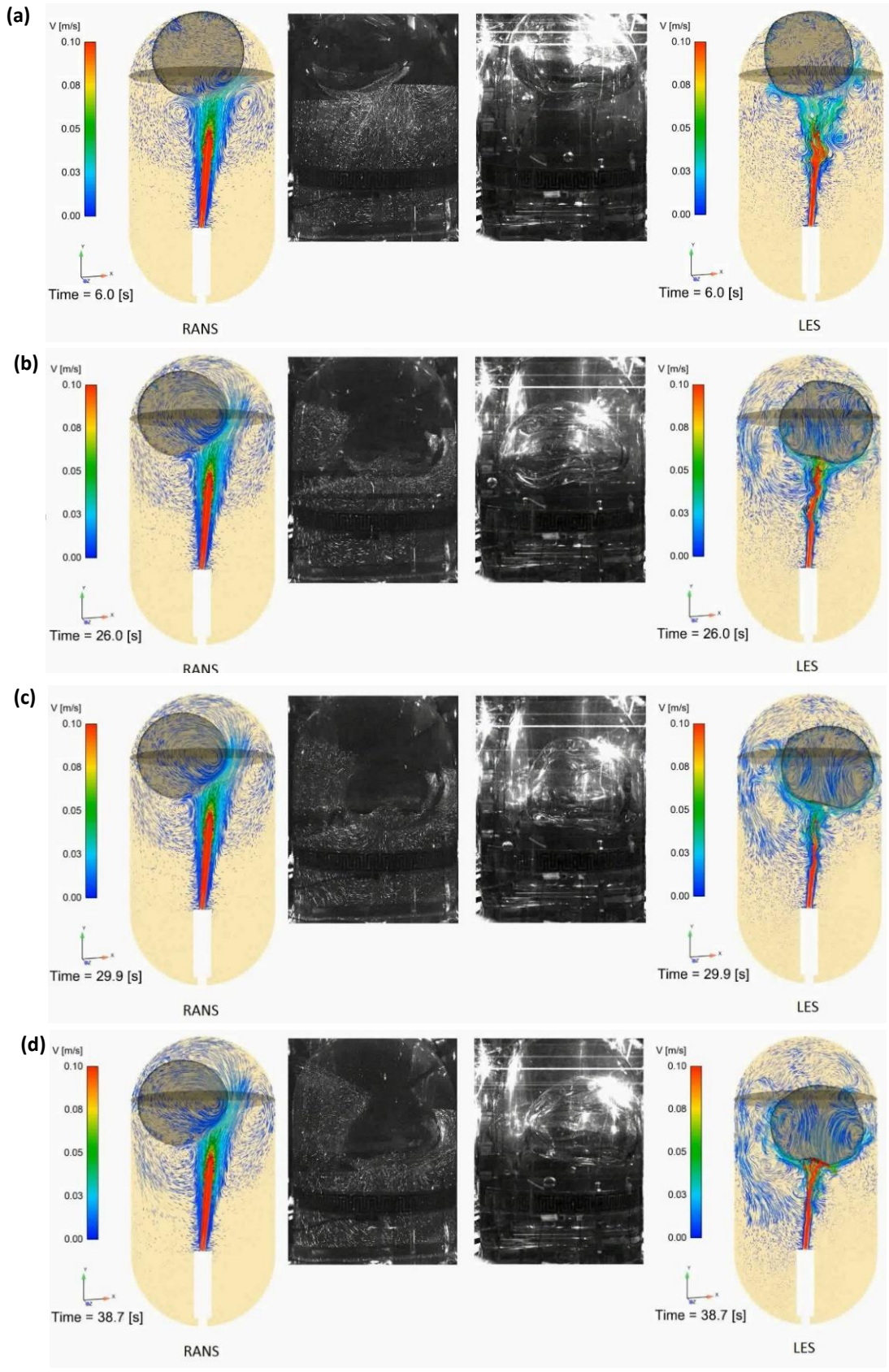


Figure 14: ZBOT subcooled jet mixing pressure control. Comparison between the predicted evolution of fluid flow and ullage deformation and movement by the 3D VOF-CFD model using LES and RANS-SST turbulent submodels and their experimental white light and particle streak image counterparts during forced jet mixing pressure control in microgravity by a 10 cm/sec (T_o-1) subcooled jet flow in a 91% filled tank.

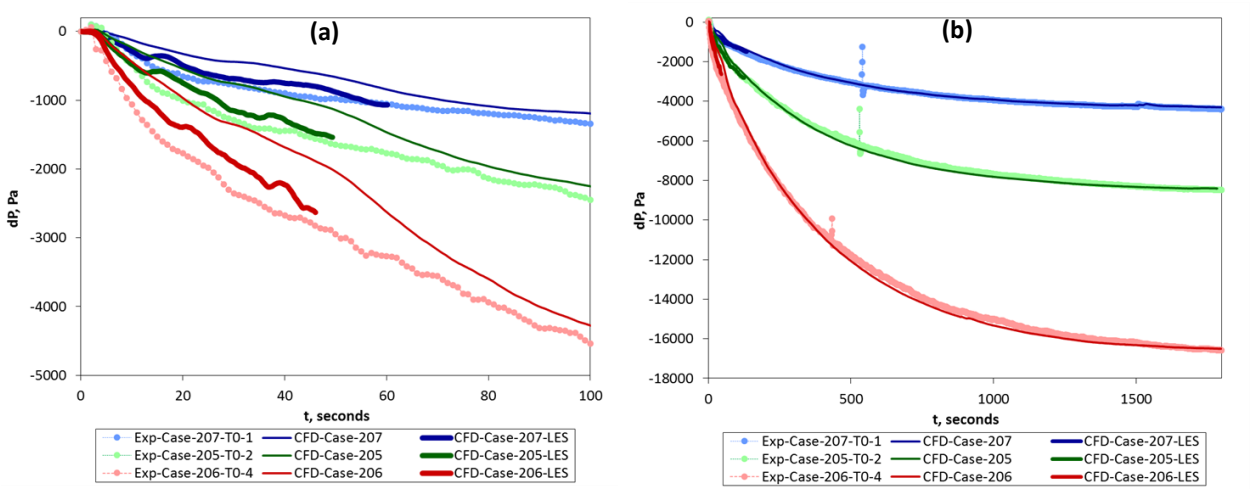


Figure 15: ZBOT subcooled jet mixing pressure control in microgravity. Comparison of the predicted short-term (a) and long-term (b) evolution of tank pressure by the 3D LES and RANS VOF-CFD models against their experimental counterparts for a 10 cm/sec (T_o-1) subcooled jet flow in a 91% filled tank in microgravity.